

Constraining the effects of dynamic topography on the development of Late Cretaceous Cordilleran foreland basin, western United States

Zhiyang Li† and Jennifer Aschoff

Department of Geological Sciences, University of Alaska, Anchorage, Alaska 99508, USA

ABSTRACT

Dynamic topography refers to the vertical deflection (i.e., uplift and subsidence) of the Earth's surface generated in response to mantle flow. Although dynamic subsidence has been increasingly invoked to explain the subsidence and migration of depocenters in the Late Cretaceous North American Cordilleran foreland basin (CFB), it remains a challenging task to discriminate the effects of dynamic mantle processes from other subsidence mechanisms, and the spatial and temporal scales of dynamic topography is not well known. To unravel the relationship between sedimentary systems, accommodation, and subsidence mechanisms of the CFB through time and space, a high-resolution chronostratigraphic framework was developed for the Upper Cretaceous strata based on a dense data set integrating >600 well logs from multiple basins/regions in Wyoming, Utah, Colorado, and New Mexico, USA. The newly developed stratigraphic framework divides the Upper Cretaceous strata into four chronostratigraphic packages separated by chronostratigraphic surfaces that can be correlated regionally and constrained by ammonite biozones. Regional isopach patterns and shoreline trends constructed for successive time intervals suggest that dynamic subsidence influenced accommodation creation in the CFB starting from ca. 85 Ma, and this wave of subsidence increasingly affected the CFB by ca. 80 Ma as subsidence migrated from the southwest to northeast. During 100-75 Ma, the depocenter migrated from central Utah (dominantly flexural subsidence) to north-central Colorado (dominantly dynamic subsidence). Subsidence within the CFB during 75-66 Ma was controlled by the combined effects of flexural subsidence induced by local Laramide uplifts and dynamic subsidence. Results from this study provide

†zli20@alaska.edu.

GSA Bulletin;

new constraints on the spatio-temporal footprint and migration of large-scale (>400 km × 400 km) dynamic topography at an average rate ranging from ~120 to 60 km/m.y. in the CFB through the Late Cretaceous. The wavelength and location of dynamic topography (subsidence and uplift) generated in response to the subduction of the conjugate Shatsky Rise highly varied through both space and time, probably depending on the evolution of the oceanic plateau (e.g., changes in its location, subduction angle and depth, and buoyancy). Careful, high-resolution reconstruction of regional stratigraphic frameworks using three-dimensional data sets is critical to constrain the influence of dynamic topography. The highly transitory effects of dynamic topography need to be incorporated into future foreland basin models to better reconstruct and predict the formation of foreland basins that may have formed under the combined influence of upper crustal flexural loading and dynamic subcrustal loading associated with large-scale mantle flows.

1. INTRODUCTION

Foreland basins, which form along convergent plate boundaries, are among the largest accumulations of sediment on Earth (DeCelles, 2012). All foreland basins ultimately owe their existence to flexural subsidence in response to loading by the adjacent thrust belt. In retroarc foreland basins, formed on an overriding plate in rapidly converging oceanic-continental subduction regimes, mantle-driven dynamic subsidence provides an additional basin-scale subsidence mechanism (Mitrovica et al., 1989; Gurnis, 1992; Shephard et al., 2010; Flament et al., 2013). At present, most foreland basin models emphasize the importance of subsidence caused by upper crustal processes, yet subcrustal processes such as mantle flow related to subduction are also important but are poorly understood.

The Cretaceous North American Cordilleran foreland basin (CFB) is one of the best-dated and

the most extensively studied retroarc foreland basins in the world. Within the CFB, short-wavelength (within ~200-300 km) flexural subsidence due to loading of the Sevier fold-and-thrust belt is relatively well understood and has been considered the dominant mechanism responsible for the rapid subsidence close to the orogenic belt (Jordan, 1981; Pang and Nummedal, 1995; DeCelles, 2004). Flexural subsidence alone, however, cannot fully explain the regional subsidence in the CFB far eastward of the Sevier orogenic belt (Painter and Carrapa, 2013; Liu et al., 2011, 2014). Instead, dynamic subsidence has increasingly been invoked to account for the long-wavelength (~1000 km) subsidence within the CFB because stresses induced by mantle flows can translate over much larger distances (Mitrovica et al., 1989; Gurnis, 1992; Catuneanu et al., 1997).

Geodynamic models have linked the broader subsidence in the CFB to the low-angle to flat subduction of an oceanic plateau—the conjugate Shatsky Rise-on the oceanic Farallon plate (Liu et al., 2010). Recent advances in seismic tomography and inverse modeling have allowed modeling of dynamic effects on subsidence during the Late Cretaceous based on the presumed current location of the Farallon plate, plate motion rates, and mantle viscosities (Liu et al., 2008; Spasojević et al., 2009; Liu et al., 2011; Humphreys et al., 2015). Despite differences in details, several models have indicated that the conjugate Shatsky Rise, if it existed, would have collided with North America near what is now southern California, USA sometime between 90 and 85 Ma and generally moved in a northeast arcuate path across the Colorado Plateau, Colorado Rocky Mountains, and the Great Plains between 84 and 65 Ma (Fig. 1; Liu et al., 2010; Humphreys et al., 2015). The subduction of a low-density oceanic plateau (i.e., the conjugate Shatsky Rise) is thought to have played a major role in the development of the flat subduction of the Farallon plate starting at ca. 90 Ma (Liu et al., 2008; Liu and Currie, 2016). Most models predicted a broad zone of dynamic

 $https://doi.org/10.1130/B35838.1; 9 \ figures; 1 \ table; 1 \ supplemental \ file.$

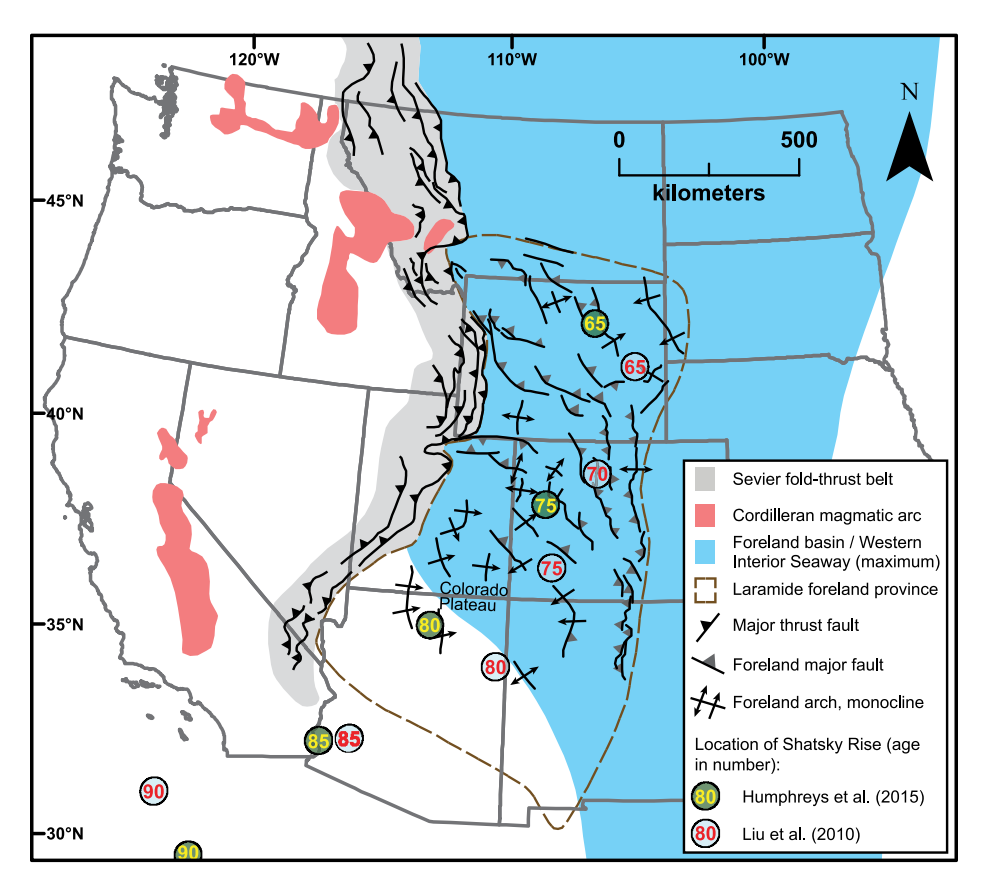


Figure 1. Regional index map of the western USA including the Sevier fold-thrust belt, Laramide province, and Cordilleran magmatic arc (modified from DeCelles, 2004; Yonkee and Weil, 2015). Approximate locations of the conjugate Shatsky Rise during 90–65 Ma from Humphreys et al. (2015) and Liu et al. (2010) are shown.

subsidence above the leading part of the Farallon plate, where both the negative buoyancy of the flat slab (due to older age or eclogitization of the basaltic crust) and magnitude of dynamic coupling between the mantle and the lithosphere would be the greatest (Mitrovica et al., 1989; Liu et al., 2010; Liu et al., 2011; Heller and Liu, 2016). The lithosphere above the trailing part of the conjugate Shatsky Rise, however, would experience much less dynamic subsidence (or even uplift) due to reduced negative buoyancy (younger in age) and less dynamic coupling (Liu et al., 2010; Heller and Liu, 2016).

Dynamic subsidence is generally considered to be an important driver of the broadening and migration of the primary depocenter in the CFB during the Late Cretaceous. Previous work that demonstrated the importance of dynamic subsidence largely relied on isopach maps and 1-D/2-D backstripping exercises to allude to the effects of dynamic subsidence/topography (Liu et al., 2010; DeCelles, 2004; Painter and Carrapa, 2013; Heller and Liu, 2016). Furthermore, some authors suggested that stratigraphic architecture (Aschoff, 2008), and fluvial and marine shore-

line depositional systems recorded the migration of dynamical subsidence/topography in the CFB (Aschoff, 2014; Heller and Liu, 2016). Yet, these independent methods have not been integrated leaving several unresolved issues.

Two key issues regarding the role of dynamic topography (including both uplift and subsidence) in the CFB remain unsolved: (1) the exact trajectory, footprint, and rate of migration of dynamic topography in the CFB associated with the subduction of the conjugate Shatsky Rise and (2) disentangling the dynamic versus flexural components on basin development. The numerical modeling of the subsidence associated with dynamic mantle processes was inevitably limited by many inherent uncertainties in solid-earth parameters, such as the viscosity and thermal structure of the mantle and the history of mantlesurface interactions (Liu et al., 2008; Flament et al., 2013). Consequently, results from different models of dynamic subsidence departed in detail (Liu et al., 2010; Humphreys et al., 2015), and need to be independently verified based on comparison with regional geology (Painter and Carrapa, 2013; Liu et al., 2014; Heller and Liu,

2016). However, because previous efforts to reconstruct the geohistory (i.e., subsidence and uplift) in the CFB were commonly based on onedimensional or two-dimensional data sets (e.g., well logs, stratigraphic sections, or regional cross-sections) or rare three-dimensional data sets with widely scattered control points (e.g., Roberts and Kirschbaum, 1995; Painter and Carrapa, 2013; Liu et al., 2014), it is not always straightforward to discriminate subsidence generated by dynamic mantle processes from offaxis flexural subsidence (e.g., due to loading of local Laramide uplifts). Without a detailed stratigraphic analysis over a sufficiently large area and in a three-dimensional context, the spatial variability in the tectonic history (uplift and subsidence) across the CFB may have been significantly underestimated, posing additional challenges to constraining the effects of dynamic topography and discriminate different subsidence mechanisms.

The primary goal of this study is to identify and characterize the effects of dynamic subsidence (and uplift) based on a higher-resolution, more comprehensive reconstruction of the geological history of the CFB that integrates variability in the stratigraphic architecture, stratal thickness trends, and shoreline orientations with a robust age control. To do this, we built a detailed chronostratigraphic framework for the CFB based on high-resolution ammonite zonations and sequence stratigraphy, and reconstructed the distribution of sedimentary systems and sediment accumulation within the foreland basin based on regional stratigraphic correlations. This work differs from previous studies (e.g., Jones et al., 2011; Painter and Carrapa, 2013) in two key ways—correlations are based on: (1) chronostratigraphic surfaces (i.e., time lines) carefully constrained by detailed and most updated ammonite zones and sequence stratigraphic concepts and (2) much denser control points including more than 600 geophysical well logs from multiple basins in the central part of the CFB (Wyoming, Utah, Colorado, and New Mexico). To provide critical new detail in the stratigraphic interval that records dynamic subsidence migration we specifically focus on the Late Cretaceous (from ca. 100 Ma to 66 Ma). During this time dynamic subsidence was presumed to migrate across interior North America in response to the shallow subduction of the postulated conjugate Shatsky Rise on the Farallon plate, although the exact track is debated (Liu et al., 2010; Humphreys et al., 2015). This study defines four depositional packages within Upper Cretaceous strata of the CFB and presents isopach maps with general shoreline trends to delineate the spatio-temporal pattern of dynamic subsidence migration. Improved understanding of the distribution of sedimentary systems and migration of depocenters in the CFB across space and time could help discriminate the effects that crustal and subcrustal loading had on the basin dynamics of the CFB. By integrating the newly developed isopach patterns, recently reconstructed shape and path of the conjugate Shatsky Rise beneath North America (Liu et al., 2010; Humphreys et al., 2015), and timing of initiation of Laramide structures (DeCelles, 2004; Yonkee and Weil, 2015; Heller and Liu, 2016), the effects of subcrustal mantle flows on the subsidence in retroarc foreland basins can be better constrained. This can provide useful insights for future modeling of dynamic subsidence in foreland basins formed in other oceanic-continental convergent systems.

2. GEOLOGIC CONTEXT

The geology of western North America was largely controlled by the subduction of the Farallon plate beneath the North American plate during Jurassic to Paleogene time. The compressive forces associated with plate convergence, combined with conductive heating initiated by subduction, led to crustal thickening in orogenic belts such as the Sevier fold-and-thrust belt (Livaccari 1991; DeCelles, 2004). During the Late Jurassic and Cretaceous, the Western Interior of North America was occupied by a broad retroarc foreland basin (i.e., the CFB) that developed on the eastern margin of the Sevier thrust belt in response to combined flexural loading from the Sevier orogenic belt and dynamic subsidence associated with flab slab subduction of the Farallon plate (Fig. 1). The subsidence of the CFB during the Late Cretaceous is thought to mark a critical transition from flexural to dynamic subsidence, and several studies have suggested that dynamic subsidence migrated across the western United States in response to subduction of the conjugate Shatsky Rise on the Farallon plate during this time (Liu et al., 2010; Heller and Liu, 2016). Consequently, the spatiotemporal subsidence history of the interplay of flexure and dynamic subsidence is recorded by the Late Cretaceous strata that are the focus of this study.

Late Cretaceous subsidence in the CFB is generally considered to have occurred in three distinct phases. During Cenomanian to Coniacian time, the CFB was characterized by a narrow, deep depocenter adjacent to the Sevier orogenic belt (DeCelles, 2004). Starting in the Santonian, the isopach pattern characteristic of flexural subsidence becomes diffuse. By early Campanian, the depocenter in the CFB became broader and migrated away from the thrust front, indicating a greater component of long-wavelength dynamic

subsidence induced by large-scale mantle down-welling flows associated with the flat subduction of the Farallon slab under North America (Mitrovica et al., 1989; Pang and Nummedal, 1995; Catuneanu et al., 1997; Liu et al., 2011; Painter and Carrapa, 2013). Beginning at the Late Campanian (ca. 75 Ma) to Maastrichtian, the foreland basin became partitioned by intraforeland Laramide-style basement-cored uplifts (Fig. 1), among which local depocenters started to form and disrupt the regional subsidence pattern in the CFB (Dickinson et al., 1988; DeCelles, 2004; Lawton, 2008; Jones et al., 2011).

The combined effects of flexural loading, dynamic subsidence, and global eustatic high throughout the Late Cretaceous resulted in the development of an epicontinental seaway known as the Western Interior Seaway (WIS; Kauffman, 1977, 1985). The most extensive flooding of the seaway occurred in the early Turonian, when the WIS extended from the Arctic Ocean to the Gulf of Mexico, and more than one-third of North America was inundated (Fig. 1). Deposition during the early Late Cretaceous was characterized by fully marine to marginal marine systems fed by non-marine feeder systems derived from the Sevier fold-and-thrust belt to the west. Following the peak Turonian transgression to Maastrichtian, the WIS was subject to at least four secondorder (2-10 m.y. duration sensu Mitchum and Van Wagoner, 1991) regressive-transgressive marine cycles, but gradually retreated from the continental interior and drained northward into Canada and southward into Texas, USA. The withdrawal of the WIS led to the east- to northeast-directed progradation of marine shorelines and more widespread nonmarine sedimentation in the foreland basin as nonmarine systems fed these prograding shorelines.

3. METHODOLOGY AND RATIONALE

3.1. Chronostratigraphic Framework and Correlation Criteria

The abundance of well logs and numerous previous stratigraphic studies across the CFB allow the reconstruction of the geological history in our study area (Fig. 2) with excellent temporal constraints. A comprehensive chronostratigraphic and biostratigraphic framework of Upper Cretaceous strata of different basins/regions in our study area was first developed based on compilation of numerous previous studies (Fig. 3). The geologic time scale used in this study is from Gradstein et al. (2012). Cobban et al. (2006) first defined Cretaceous Western Interior ammonite biozones, the ages of which were updated in Ogg et al. (2012). Geochronologic data (e.g., ⁴⁰Ar/³⁹Ar and detrital zir-

con U-Pb radiometric ages) available in certain basins/regions provide additional temporal constraints for some lithostratigraphic units in these areas. Sources for developing the time-space correlation of Upper Cretaceous stratigraphic units in Utah, Colorado, and the northern part of New Mexico are compiled and summarized in Table S1¹ in the Supplemental Material. A similar chronostratigraphic and biostratigraphic framework of Upper Cretaceous strata of different basins/regions in Wyoming was developed by Lynds and Slattery (2017) and is directly used herein.

The data set for this study is vastly expanded from previous work (e.g., Roberts and Kirschbaum, 1995; Jones et al., 2011; Painter and Carrapa, 2013), and it builds on several subregional studies (Kirschbaum and Hettinger, 2004; Aschoff, 2008; Edwards, 2011; Rountree, 2011; Daniele, 2012; Wiechman, 2013; Rust, 2019). A total of 627 geophysical well logs (with gamma ray, spontaneous potential, and conductivity curves) from multiple basin and regions in Wyoming, Utah, Colorado, and New Mexico were used (Fig. 2). Of all the well logs, 260 contain the entire Late Cretaceous (Cenomanian to Maastrichtian) interval. The tops of all formations (and distinct members) of Late Cretaceous age in each well were picked in IHS Petra. Additionally, five chronostratigraphic surfaces (time lines) were selected based on the developed chronostratigraphic and biostratigraphic framework to divide Upper Cretaceous strata in our study areas into four stratigraphic packages (Fig. 3). The most important selection criterion for these surfaces is that these surfaces (biozone boundaries) can be confidently correlated across all basins/regions in the study area. These surfaces include: base of Cenomanian (100.5 Ma), top of biozone Scaphites whitfieldi (90.24 Ma), top of biozone Baculites maclearni (80.21 Ma), top of biozone Exiteloceras jenneyi (74.6 Ma), and top of Maastrichtian (66 Ma). The numerical ages for each biozone boundary were assigned based on the Cretaceous time scale from Ogg et al. (2012). It is critical to highlight that, however, the absolute ages of some lithostratigraphic units and in the Cretaceous time scale are likely to be updated when more precise age data become available, which could potentially require modification of the stratigraphic correlation based on numerical ages (e.g., ages from geochronological dating). To avoid this problem, ammonite

¹Supplemental Material. Tables S1 and S2. Table S1 includes sources for the chronostratigraphic framework in Figure 3 and Table S2 includes information of well logs shown in Figure 4. Please visit https://doi.org/10.1130/GSAB.S.14384429 to access the supplemental material, and contact editing@geosociety.org with any questions.

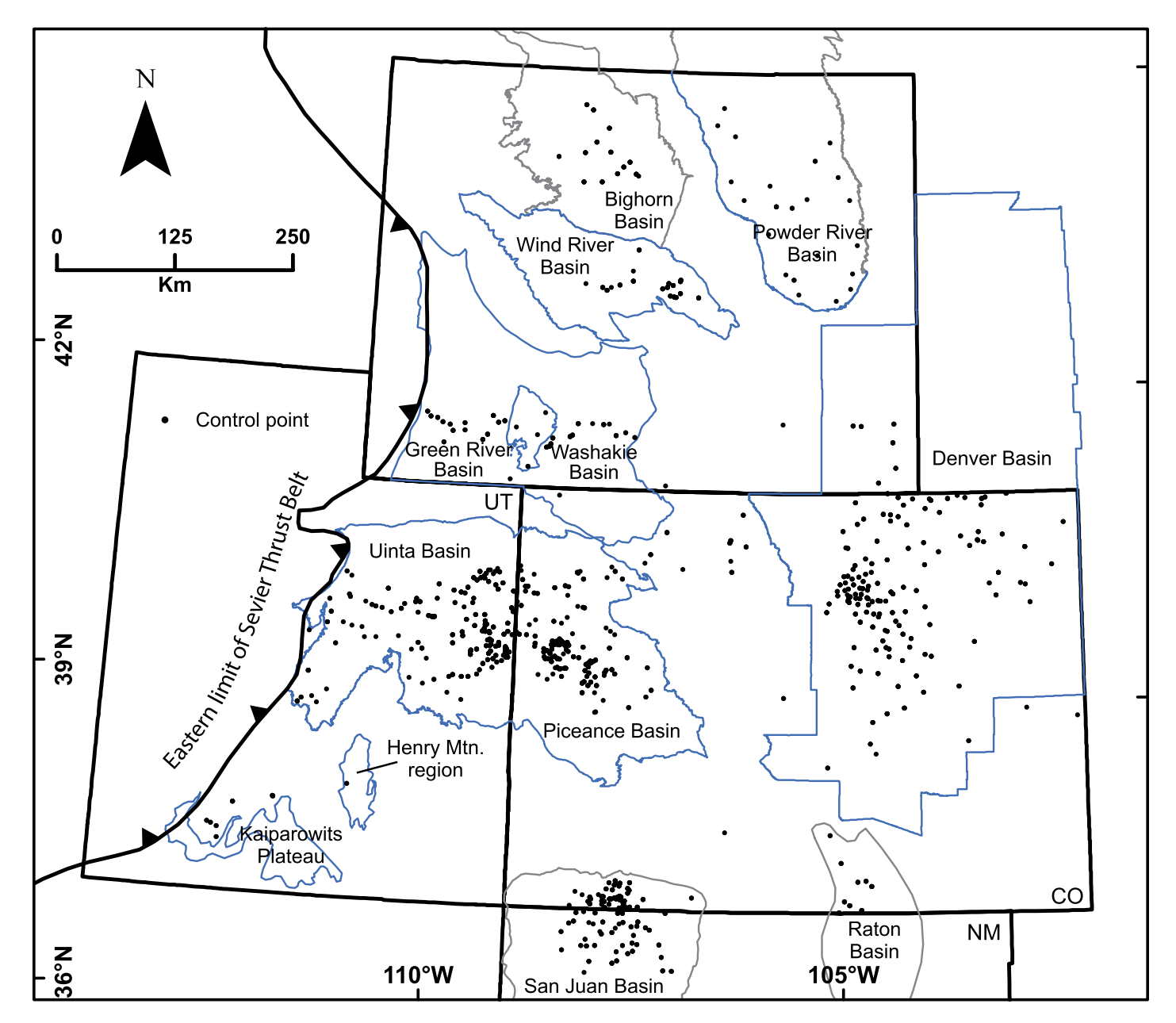


Figure 2. Map showing locations of well log control points from multiple basins and regions in the study area in the North American Cordilleran foreland basin, western United States. Mtn.—Mountains.

biozones, rather than absolute ages, were used as the first-order temporal constraints for all the selected chronostratigraphic surfaces. In other words, as long as the same ammonite biozone boundaries were correctly picked and correlated, the stratigraphic correlation and developed isopach patterns from this study will remain valid, and the assigned ages for our selected biozone boundaries (time lines) can simply be updated with the newest time scale.

To ensure that the same chronostratigraphic surfaces (i.e., time lines) were systematically chosen, detailed criteria used to pick all selected biozone boundaries at different basins/regions were carefully compiled from a large number of detailed biostratigraphic studies (Table 1). Although biostratigraphic data are not available for all well logs within the data set, each basin/region has at least one region that has robust biostratigraphic control from outcrop or core. Well logs containing the same surfaces (i.e., biozone boundaries) picked by earlier studies were verified and incorporated into our data set, and these served as control points in our stratigraphic framework (Table 1). Sequence stratigraphic concepts were used to subsequently correlate selected chronostratigraphic surfaces throughout each basin/region. It is important to note, how-

ever, that the same chronostratigraphic surface is likely to be characterized by different lithostratigraphic or sequence stratigraphic relationships across different basins/regions because different areas within the CFB may experience uplift or subsidence at the same time (Table 1). The correlation of five chronostratigraphic surfaces across several type logs from different basins/regions in Utah, Colorado, and New Mexico is shown in Figure 4. After the correlation was done in IHS Petra, the thickness between selected chronostratigraphic surfaces can be exported as XY grids. These grids were then imported into Arc-GIS to generate contours. Four isopach maps

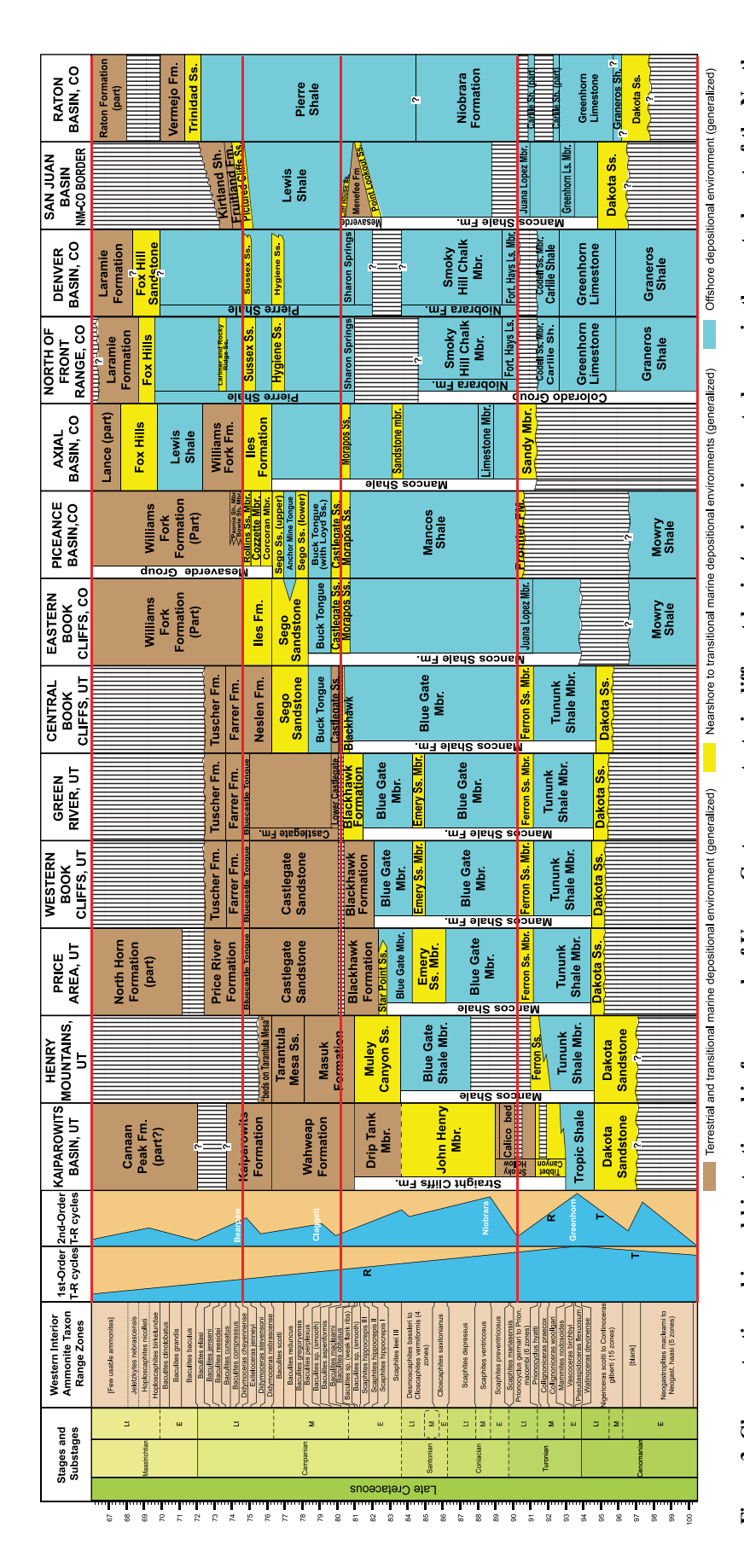


Figure 3. Chronostratigraphic and biostratigraphic framework of Upper Cretaceous strata in different basins/regions in our study area in the central part of the North American Cordilleran foreland basin, western United States. Red lines indicate the chronostratigraphic surfaces used to develop isopach maps in this study. References for Early; Fm.—Formation; Mbr.—Member; Ss.—Sandstone; Sh.—Shale; Ls.—Limestone; UT—Utah; CO—Colorado; NM—New Mexico; T—transgression; R—regression. constructing the stratigraphic column at each location are compiled and summarized in Table S1 in the Supplemental Material (see footnote 1). Lt—Late; M—Middle; E—

spanning ca. 100–90 Ma, 90–80 Ma, 80–75 Ma, and 75–66 Ma were produced.

3.2. Discriminating Different Subsidence Mechanisms

Accommodation is the space made available for potential sediment accumulation, by sea-level rise, subsidence, or a combination of these two processes (Jervey, 1988; Posamentier et al., 1988). Because the contribution of eustasy to accommodation in the Late Cretaceous CFB is comparatively much smaller (<200 m), the accommodation creation within the CFB is on the first-order controlled by subsidence (Jordan, 1981; Shanley and McCabe, 1994). In this sense large scale patterns of sediment accumulation can be used as a proxy for subsidence. Different subsidence mechanisms in the CFB can be resolved by integrating the newly developed isopach patterns with comprehensive reconstructions of the geological history of the CFB. The wavelength of subsidence is the most important criterion to discriminate between flexural subsidence and dynamic subsidence (Burgess and Moresi, 1999). Flexural loading of the thrust belt typically creates short-wavelength (<200 km) subsidence close to the orogenic belt. A generic foreland basin developed under the dominant flexural subsidence contains wedge top, foredeep, forebulge, and back-bulge depozones (DeCelles and Giles, 1996). In contrast, depocenters created by dynamic mantle flows are typically broad and long-wavelength (>500 km), which may modify or even obliterate the well-organized flexural foreland basin geometry (Burgess and Moresi, 1999; DeCelles, 2012; Tufano and Pietras, 2017). To exclude effects of flexural subsidence produced by the Sevier fold-and-thrust belt and local Laramide uplifts, the timing and location of active Sevier thrusts and Laramide structures were compiled from various previous studies (Dickinson et al., 1988; DeCelles, 2004; Yonkee and Weil, 2015; Heller and Liu, 2016) and plotted on the isopach map of the corresponding time interval. To examine the effects of the conjugate Shatsky Rise on dynamic subsidence within the CFB, recently reconstructed locations of the conjugate Shatsky Rise (Liu et al., 2010; Humphreys et al., 2015) were overlain on isopach maps starting from 80 to 66 Ma, during which time the oceanic plateau was presumed to migrate across the study area.

Two factors may complicate the interpretation of subsidence from isopach maps constructed herein. First, depending on the location within the basin or depositional environments, accommodation can be overfilled or underfilled. For sedimentary basins (e.g., CFB) connected to the global ocean, accommodation is

TABLE 1. CRITERIA TO PICK CHRONOSTRATIGRAPHIC SURFACES ACROSS DIFFERENT BASINS/REGIONS IN OUR STUDY AREA. NORTH AMERICAN CORDILLERAN FORELAND BASIN. WESTERN UNITED STATES

Basin/region	Stratigraphic location	Notes and references
-	On angraphic location	140tes and references
<u>Cretaceous—Paleogene boundary: 66 Ma</u> Green River, Wind River, Bighorn, and Powder River Basins, WY	Top of Lance Fm	Connor (1992); Merewether (1996); Finn and Johnson (2005); Finn (2007); Finn (2010); Lynds and Slattery (2017)
Wasatch Plateau (west of San Ranfael Swell), UT	Top of lower North Horn Fm	Lawton (1986)
East of San Ranfael Swell in Uinta Basin, UT	Top of Price River or Tusher Fm	Lawton (1986)
Kaiparowits Plateau, UT Piceance Basin, CO	Top of Canaan Peak Fm In Upper Williams Fork Fm	Roberts et al. (2005) Used base of WF600 in Patterson et al. (2003);
Ticeance basin, GO	in Opper Williams Fork Fin	Laskowski et al. (2013)
Denver Basin, CO	Top of Laramie Fm in Denver Basin	Anna (2012)
San Juan Basin, NM and CO	Top of Kirkland Shale (base of Ojo Alamo)	Molenaar et al. (2002)
Raton Basin, CO	Top of Vermejo Fm	Molenaar et al. (2002)
Top of Exiteloceras jenneyi (late Campanian): 74.6 Ma		
Bighorn Basin, southwestern Powder River Basin, and	SB at the base of Teapot Sandstone Mbr of	Merewether (1996); Finn (2007); Finn (2010);
Wind River Basin, WY Green River Basin, WY	Mesaverde Fm SB at the base of Canyon Creek or Pine	Lynds and Slattery (2017) Finn and Johnson (2005); Lynds and Slattery (2017)
Green river basin, vv i	Ridge Sandstone Mbr	Tillit and Johnson (2005), Lyrius and Stattery (2017)
Western to central Uinta Basin, UT	Top of Bluecastle Fm	Fouch et al. (1983); Lawton (1986); Hampson et al. (2005);
		Aschoff and Steel (2011)
Eastern Uinta Basin, UT	Top of Neslen Fm	Fouch et al. (1983); Kirschbaum and Hettinger (2004);
Kaiparowits Plateau, UT	Top of middle unit of Kaiparowits Fm	Anna (2012) Roberts (2007); Lawton and Bradford (2011)
Piceance Basin, CO	FS on top of Rollins Sandstone	Schwendeman (2011)
Denver Basin, CO	FS on top of Terry (Sussex) Ss. in Pierre	Izett et al. (1971); Anna (2012)
Com Ivan Books CO	Shale	Malanana and Daird (1000). M. L (2005)
San Juan Basin, CO San Juan Basin, NM	Base of Pictured Cliffs FS on top of Pictured Cliffs	Molenaar and Baird (1989); Molenaar et al. (2002) Molenaar and Baird (1989); Fassett (2010)
Raton Basin, CO	Top of Sussex-equivalent	Projected from well logs in the Denver Basin
,	.,	.,
Top of Baculites maclearni (middle Campanian): 80.21 Ma Bighorn Basin. WY	Close to the top of Cody Shale	Time transgressive. Finn (2010); Lynds and Slattery (2017)
Southwestern Powder River Basin, WY	In the upper part of Steele Shale Mbr of Cody	Merewether (1996); Lynds and Slattery (2017)
,	Shale	
Eastern Wind River Basin, WY	Top of a sandstone member in Upper Cody	Finn (2007); Lynds and Slattery (2017)
Eastern and Southern Rock Spring Uplift, WY	Shale In the upper part of Rock Springs Fm	Finn and Johnson (2005); Lynds and Slattery (2017)
Washakie Basin. WY	In the lower part of Haystack Mtns Fm	Finn and Johnson (2005); Lynds and Slattery (2017)
Western to central Uinta Basin	Base of Castlegate (sequence boundary)	Lawton (1986); Franczyk et al. (1990); Elder and Kirkland
Forton Histo Books to Biocomos Books HT to CO	FO above Marrage Oa	(1994); Robinson and Slingerland (1998)
Eastern Uinta Basin to Piceance Basin, UT to CO Kaiparowits Plateau, UT	FS above Morapos Ss Top of lower Wahweap	McGookey et al. (1972); Schwendeman (2011) FS (base level rise). Jinnah and Roberts (2011);
raiparowno i latoau, o i	Top of lower warmeap	Mulhern and Johnson (2017)
Henry Mountains Region, UT	Top of lower Masuk	FS (base level rise). Corbett et al. (2011)
Denver Basin, CO	Top of Sharon Springs	Izett et al. (1971); McGookey et al. (1972); Tanck (1997);
San Juan Basin, NM = CO border	FS above lower Cliff House Ss	Lynds and Slattery (2017) Molenaar and Baird (1989); Molenaar et al. (2002)
Raton Basin, CO	Top of Sharon Springs (FS?)	Gill et al. (1972); Molenaar et al. (2002)
•	rop or original opinings (i. o.)	S. S. C. C. C. C. S. S. S. S. C.
Top of Scaphites whitfieldi (late Turonian): 90.24 Ma Green River, Wind River, Bighorn, and Powder River	Close to the top of Frontier Fm (SB within the	Merewether (1996); Finn and Johnson (2005); Finn (2007);
Basins	Frontier)	Finn (2010); Lynds and Slattery (2017)
Western to central Uinta Basin, UT	FS above Ferron Ss	Molenaar and Cobban (1991)
Eastern Uinta Basin, UT	Top of Juana Lopez	Molenaar and Cobban (1991)
Kaiparowits Plateau, UT	Calico SB	Shanley and McCabe (1995); Hettinger et al. (2000);
Henry Mountains Region, UT	FS above Ferron Ss	Lawton et al. (2014); Primm et al. (2018) Seymour and Fielding (2013)
Piceance Basin, CO	FS above Frontier Fm	McGookey et al. (1972); Molenaar and Cobban (1991)
Denver Basin, CO	Top of Carlile Shale	Merewether et al. (2011); Joo and Sageman (2014)
San Juan Basin, CO and NM Raton Basin, CO	Top of Juana Lopez Top of Carlile Shale	Molenaar and Baird (1989); Molenaar et al. (2002) Molenaar et al. (2002); Merewether et al. (2011)
•	TOP OF CATHIE STIAIC	wordinaar et al. (2002), welewellier et al. (2011)
Cenomanian Base: 100.5 Ma	Ton of Marrier Chala	Manage (4000), Fire and J. J. (2005), Fig. (2005)
Green River, Wind River, Bighorn, and Powder River Basins, WY	Top of Mowry Shale	Merewether (1996); Finn and Johnson (2005); Finn (2007); Finn (2010); Lynds and Slattery (2017)
Uinta Basin, UT	SB at the base of Dakota Sandstone	Molenaar and Cobban (1991)
Kaiparowits Plateau, UT	SB at the base of Dakota Sandstone	Antia and Fielding (2011); Seymour and Fielding (2013);
U. M. C. B. C. UT	00 111 1 10 10 11	Lawton et al. (2014)
Henry Mountains Region, UT Piceance Basin, CO	SB at the base of Dakota Sandstone FS above Dakota Sandstone	Antia and Fielding (2011); Seymour and Fielding (2013) Molenaar and Cobban (1991); Anna (2012)
Denver Basin, CO	Top of Mowry Shale	Higley and Schmoker (1989); Higley and Cox (2007)
San Juan Basin, CO and NM	SB at the base of Dakota Sandstone	Antia and Fielding (2011); Molenaar and Baird (1989);
Raton Basin, CO	OD at the horse of Dallack Co. 1.1	Molenaar et al. (2002)
	SB at the base of Dakota Sandstone	Molenaar et al. (2002); Bush et al. (2016)

typically overfilled in continental environments above the sea level, and underfilled in marine environments (Catuneanu, 2019). Therefore, the distribution of sediment accumulation revealed

by isopach maps need to be incorporated with the distribution of sedimentary systems (e.g., paleoshoreline locations) to correctly infer the temporal and spatial variations in the creation

(and destruction) of accommodation within the CFB. Second, the original depositional geometry may be distorted by differential compaction (Steckler and Watts, 1978). Although isopach

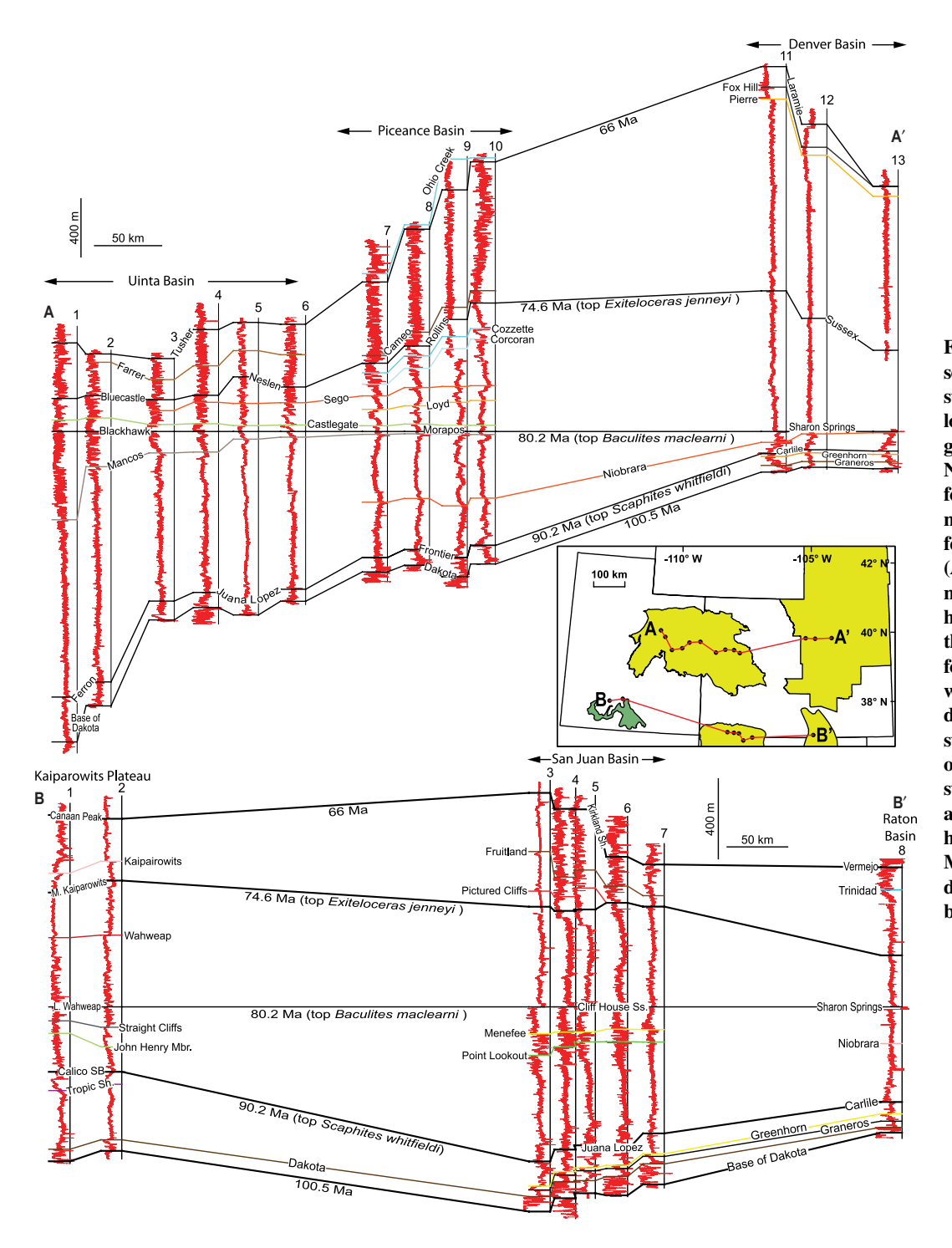


Figure 4. Correlation of five chronostratigraphic selected surfaces based on some type logs from multiple basins/regions in Utah, Colorado, and New Mexico, USA. See Table 1 for criteria to pick these chronostratigraphic surfaces in different basins/regions. The API (American Petroleum Institute) numbers of all well logs shown here can be found in Table S2 in the Supplemental Material (see footnote 1). The correlation of well logs in Wyoming was based directly on Upper Cretaceous stratigraphic framework developed by a number of previous studies (see Table 1 for sources) and therefore was not shown here. Ss-sandstone: Sh-shale: Mbr.—Member; M.—Middle; L.-Lower; SB-surface boundary.

maps constructed in this study do not show decompacted thickness, the observed isopach patterns are still considered to be reliable indicators of relative subsidence within the study area because this study focuses on the distribution and relative amount of sediment accumulation and accommodation (subsidence) over large spatial (>100 km) and temporal (>5 m.y.) scales (Chamberlain et al., 1989; Varban and Guy Plint, 2008).

4. TEMPORAL CHANGES IN ISOPACH PATTERNS WITHIN THE CFB

4.1. Cenomanian to Late Turonian (100–90 Ma) Deposition

Strata deposited during the Cenomanian to late Turonian within the CFB form part of the 2nd-order Greenhorn transgressive-regressive sea-level cycle (Fig. 3). Transgression of the

Greenhorn cycle began in the latest Albian and peaked in the early Turonian (Kauffman, 1985). As a result of the expansion of the WIS during the Greenhorn transgression, sediment fill within the CFB consists of widespread offshore (hemi-pelagic to pelagic) deposits in an openmarine environment (e.g., the Tropic Shale and the Tununk Shale Member of the Mancos Shale in Utah, the Greenhorn Formation in central and eastern Colorado; Fig. 3). The regressive phase

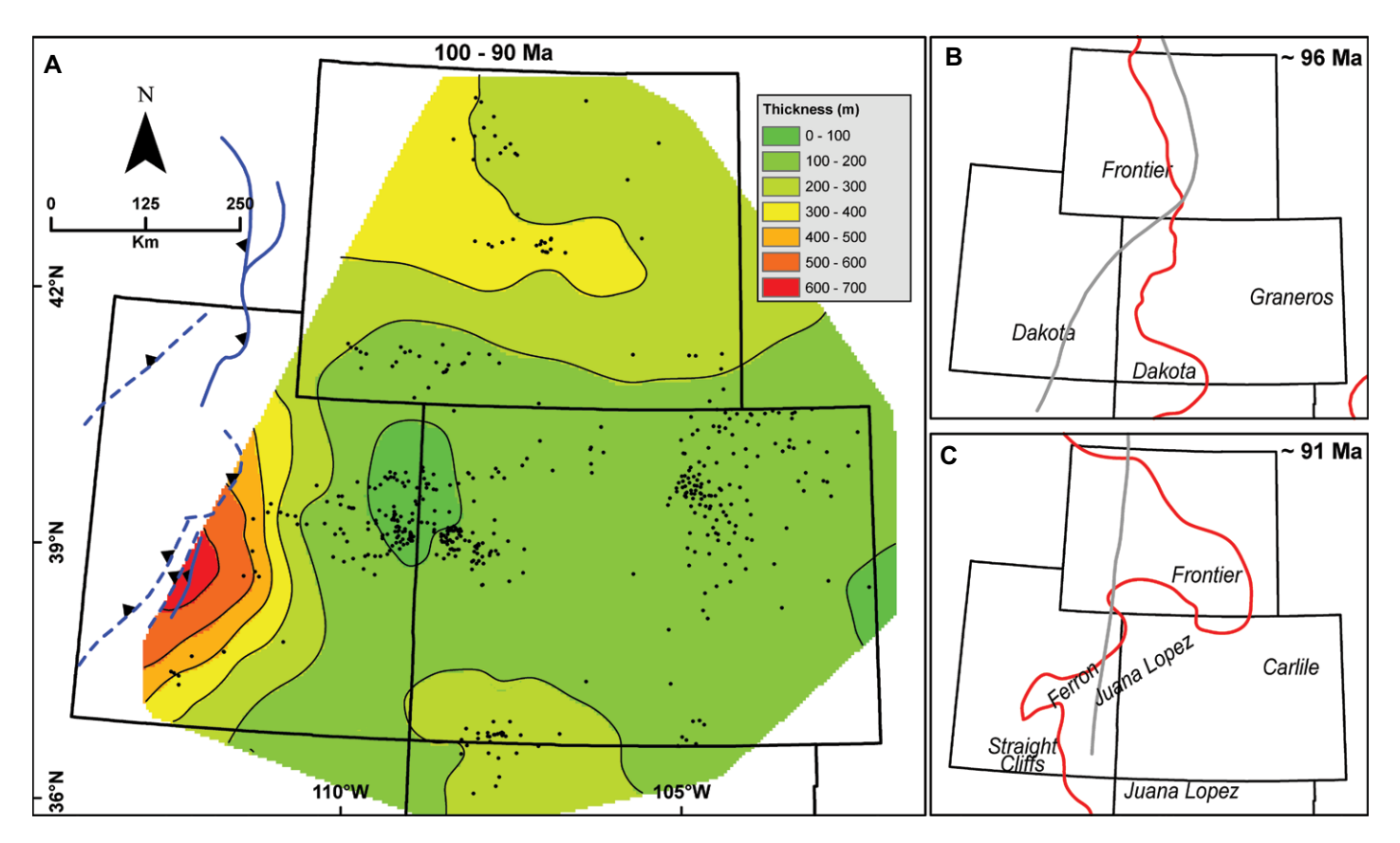


Figure 5. (A) Isopach map of Cenomanian to late Turonian (ca. 100–90 Ma) strata in the study area. Solid and dashed barbed lines indicate active and inactive thrusts, respectively (from DeCelles, 2004). Black dots represent well log control points. (B and C) are maps showing the approximate locations of the paleoshoreline (red line) and forebulge (gray line), as well as distribution of sedimentary systems (indicated by formation/member names) at ca. 96 Ma (Conlinoceras tarrantensee zone) and ca. 91 Ma (Scaphites whitfieldi zone), respectively. The paleoshoreline locations are from Blakey (2014) and the forebulge locations are from DeCelles (2004). Maps B and C have exactly the same spatial extent as map A.

of the Greenhorn cycle took place during the early to late Turonian. The culmination of the Greenhorn regression is marked by the Ferron Sandstone Member of the Mancos Shale and the Frontier Formation, which were deposited as a series of delta complexes along the western margin of the WIS (Figs. 3 and 5C).

The isopach map of Cenomanian to late Turonian strata reveals a narrow depocenter with the thickest strata (>600 m) in central Utah, less than 200 km from the thrust front (Fig. 5). Stratal thickness rapidly thins from central Utah to eastern Utah. Most of Wyoming is characterized by a broad depocenter with moderate accommodation (Fig. 5). Eastern Utah and most of Colorado show overall low sediment accumulation (<200 m), and the area with the lowest sediment accumulation rate (<10 m/ m.y., undecompacted) is located at northwestern Utah/ northeastern Colorado (Fig. 5).

Interpretation

The well-developed foredeep, forebulge, and back-bulge depozones indicated by the isopach

map (Fig. 5) suggest that development of the CFB during the Cenomanian to late Turonian was dominated by flexural subsidence in response to loading of the Sevier fold-and-thrust belt, and the influence of dynamic topography (subsidence or uplift) is negligible everywhere in the CFB prior to 90 Ma. The narrow depocenter in central Utah represents the foredeep in front of the thrust front. The rapidly thinning sediment accumulation from central to eastern Utah indicates rapid flexural subsidence in central Utah (Fig. 5). Areas with relatively low sediment accumulation (e.g., eastern Utah, northwestern Utah/northeastern Colorado, and southwestern Wyoming) roughly correspond to the location of forebulge during this time (Fig. 5; DeCelles, 2004). During the Cenomanian to late Turonian, the forebulge migrated across western Wyoming, resulting in the significant unconformity within the Frontier Formation (from early middle Cenomanian to middle Turonian: Kirschbaum and Mercier, 2013). Consequently, almost all of Wyoming lay to the east of the foredeep/ forebulge during this time (Liu et al., 2005). The relatively low accommodation and high sediment supply of the Frontier Formation allowed the Frontier delta to bypass the forebulge and prograde farther eastward (~500 km from the thrust front) into the backbulge zone (Fig. 5). Similarly, most of Colorado and northwestern New Mexico (San Juan Basin) were located at the backbulge zone at this time. Thinner strata in these areas most likely reflect limited sediment supply in hemi-pelagic to pelagic settings instead of tectonic uplift (accommodation is underfilled).

4.2. Late Turonian to Middle Campanian (90–80 Ma) Deposition

Deposition within the CFB during the late Turonian to middle Campanian was subject to the second-order Niobrara transgressive-regressive sea-level cycle (Fig. 3). Sea-level rise during the Niobrara cycle was second largest in magnitude only to the Greenhorn cycle. The Niobrara cycle is also unique in maintaining a prolonged interval of peak flooding (Fig. 3; Kauffman,

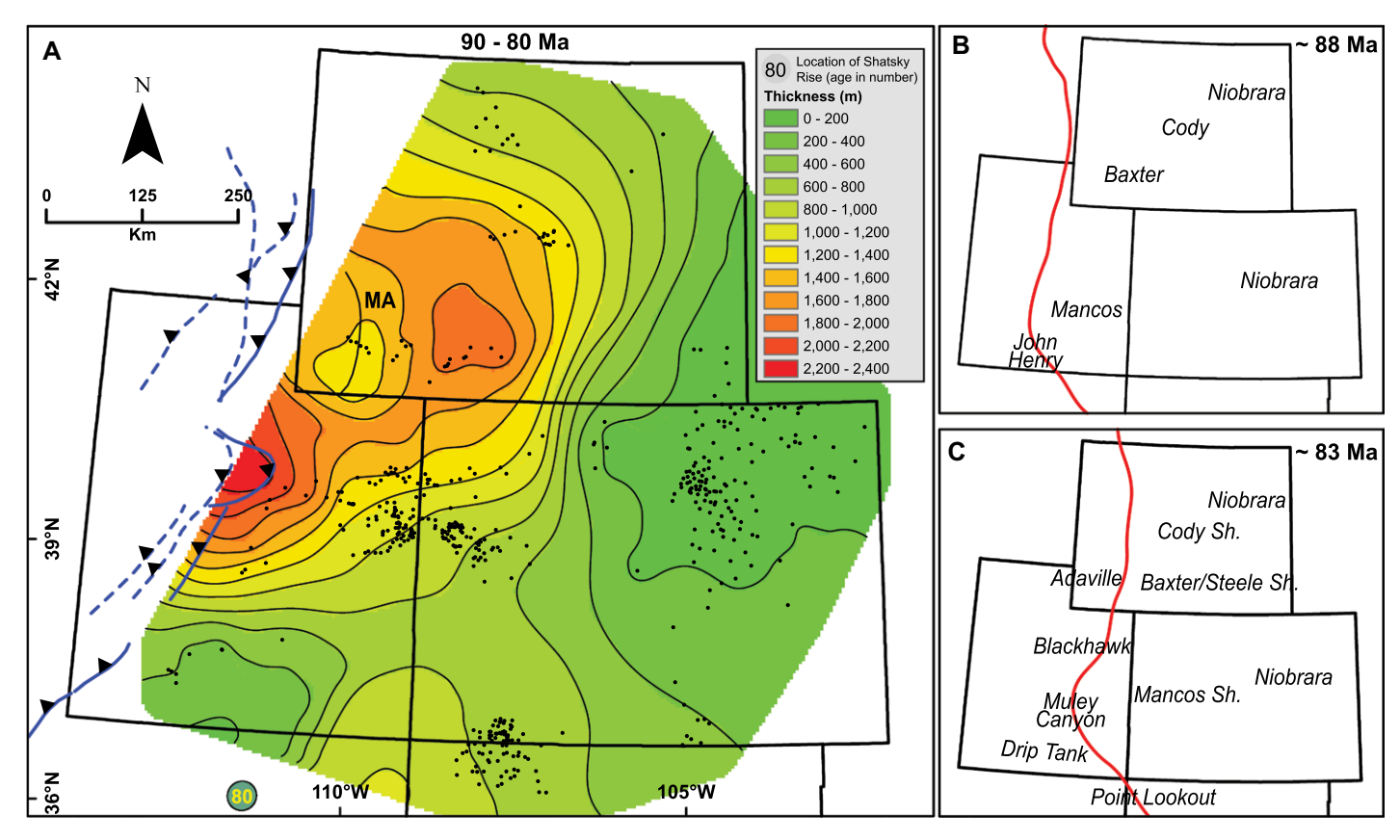


Figure 6. (A) Isopach map of late Turonian to early middle Campanian (ca. 90–80 Ma) strata in the study area. Solid and dashed barbed lines indicate active and inactive thrusts, respectively (from DeCelles, 2004). Black dots represent well log control points. (B and C) are maps showing the approximate locations of the paleoshoreline (red line) and distribution of sedimentary systems (indicated by formation/member names) at ca. 88 Ma (*Scaphites ventricosus* zone) and ca. 83 Ma (*Scaphites hippocrepis* zone), respectively. Paleoshoreline locations are from Blakey (2014). The reconstructed location of the conjugate Shatsky Rise at ca. 80 Ma is from Humphreys et al. (2015). See Figure 1 for the reconstructed location of the conjugate Shatsky Rise at ca. 80 Ma from Liu et al. (2010). Maps B and C have exactly the same spatial extent as map A. MA—Moxa Arch; Sh.—Shale.

1985), resulting in widespread, long-term deposition of offshore mudstones (e.g., Mancos Shale in Utah, western Colorado, northwestern New Mexico, Baxter/Cody Shales in western Wyoming) and marls and chalks of the Niobrara Formation (eastern Wyoming and eastern Colorado) within the CFB (Fig. 6B). Prolonged regression of the Niobrara Sea (during Santonian to early Campanian) has led to deposition of a series of eastward-prograding clastic wedges (e.g., Blackhawk Formation and Muley Canyon Sandstone in Utah) along the western margin of the WIS (Fig. 6C).

Northeastern Utah, southwestern Wyoming, and a small part of northwestern Colorado were characterized by high sediment accumulation (>1200 m) during the late Turonian to middle Campanian (Fig. 6). The overall high sedimentation of this relatively broad area is divided by the southwestern corner of Wyoming showing moderate sediment accumulation. Eastern Wyoming, central and eastern Colorado, and south-

ern Utah (northern Kaiparowits Plateau) show relatively thinner strata (<600 m) (Fig. 6). The four corners region shows slightly higher sediment accumulation rates compared to its surrounding areas (Fig. 6), despite only a limited number of control points (upper Turonian to middle Campanian strata are missing in this area due to erosion).

Interpretation

Flexural subsidence in response to loading of the Sevier thrust sheet continued to be the dominant mechanism to create accommodation and control the distribution of sediment accumulation during this time interval. The southwestern corner of Wyoming, characterized by comparatively lower sediment accumulation compared to its surrounding areas, likely represents the forebulge (Fig. 6). This is consistent with the predicted forebulge location in Wyoming (around current Moxa Arch) during this time based on three-dimensional flexural numerical modeling

(Luo and Nummedal, 2012). South of Wyoming, the forebulge is not well-defined on the isopach pattern. Nevertheless, the isopach pattern reveals a distinct foredeep showing the highest rates of sediment accumulations adjacent to the thrust front in northcentral Utah (Fig. 6). The broadening of the depocenter from northcentral Utah to northwestern Colorado (~300 km from the thrust front) is also noted in DeCelles (2004) and can be explained by an increase in rigidity of the loaded lithosphere without invoking dynamic influence (Painter and Carrapa, 2013). Different characteristics of the depocenter and forebulge between southwestern Wyoming and northeastern Utah thus likely reflect laterally variable lithospheric flexural rigidities (Tufano and Pietras, 2017).

Upper Turonian to middle Campanian strata in eastern Wyoming, as well as central and eastern Colorado, comprises marls and limestones of the Niobrara Formation. The overall low sediment accumulation of this broad area is therefore mainly due to low siliciclastic input to the hemi-pelagic to pelagic settings, similar to during the Greenhorn cycle. In contrast, sediment accumulation in proximal areas of southern Utah (Kaiparowits Plateau) should not be limited by sediment supply but by low accommodation. The relatively low accommodation in southern Utah could possibly be associated with the quiescence phase of adjacent thrusting, during which erosionally decaying loads would result in isostatic uplift of the thrust belt and foredeep. The other possible reason is related to the dynamic influence caused by the emplacement of the overall buoyant conjugate Shatsky Rise below this area by 80 Ma (Fig. 6; Humphreys et al., 2015). In this respect, the moderate accommodation at the four corners area was likely created due to the long-wavelength (~500 km) dynamic subsidence in front of the conjugate Shatsky Rise rather than flexural subsidence because the four corners area is located relatively far (>400 km) from the thrust front in southwestern Utah (Fig. 6).

4.3. Middle to Late Campanian (80–75 Ma) Deposition

Middle to upper Campanian strata within the CFB was subject to a similar 2nd-order transgressive-regressive sea-level cycle (Fig. 3; the Claggett cycle of Kauffman, 1977). Maximum flooding of this sea-level cycle was much less extensive than during the earlier Niobrara and Greenhorn cycles, which collectively mark the first-order regression of the seaway from the CFB. During the middle to late Campanian, the progressive eastward progradation of the shoreline on the western margin of the WIS led to more widespread nonmarine sedimentation in western Wyoming and eastern Utah (Fig. 7).

The Sevier fold-and-thrust sheet continued to migrate eastward during this time (Fig. 7). The conjugate Shatsky Rise was considered to have migrated from southern Utah/northern Arizona to eastern-central Colorado during 80–75 Ma (Fig. 1). Although it is generally accepted that widespread Laramide deformation did not start until ca. 75 Ma, the basement-cored Kaibab uplift

(Fig. 7), active between 80 and 76 Ma, may represent an early manifestation of Laramide deformation within the CFB (Tindall et al., 2010).

The isopach map of the middle to upper Campanian strata reveals a broad depocenter centered in northcentral Colorado (\sim 500 km from the thrust front and \sim 500 km in front of the conjugate Shatsky Rise; Fig. 7). This depocenter covers an area of \sim 500 km \times 500 km and shows >600 m sediment accumulation. Other than southern Utah (Kaiparowits Plateau region), areas close to the Sevier thrust front (western Wyoming, northeaster to central Utah) are characterized by overall low sediment accumulation (<300 m). The Kaiparowits Plateau region shows moderate to high sediment accumulation (<400–600 m).

Interpretation

Based on the predicted locations of the Shatsky Rise (Fig. 7) and the large distance (\sim 500 km) between the Sevier thrust fronts and the main depocenter during this time interval, the broad depocenter centered in northcentral Colorado is

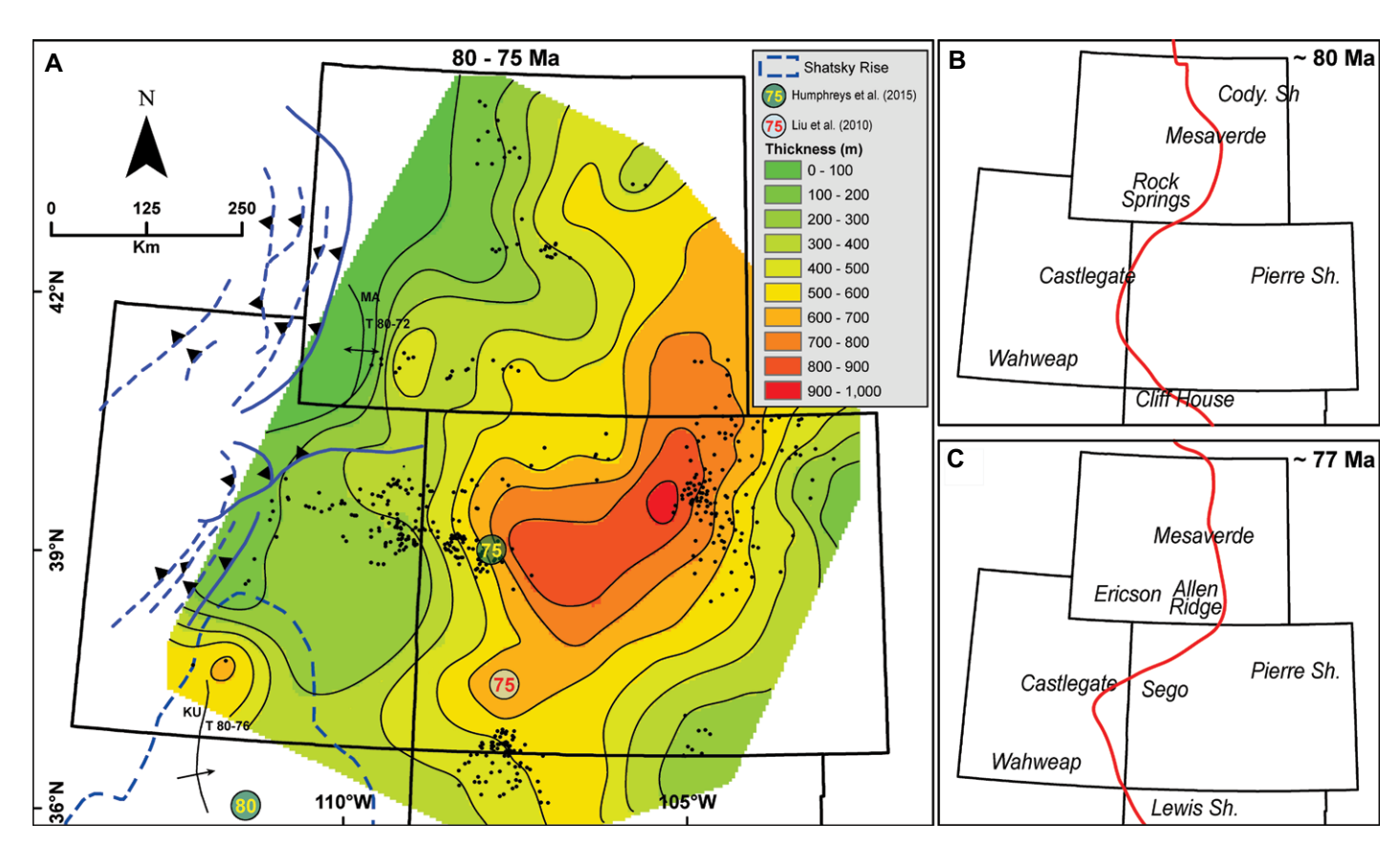


Figure 7. (A) Isopach map of middle Campanian to late Campanian (ca. 80–75 Ma) strata in the study area. Solid and dashed barbed lines indicate active and inactive thrusts, respectively (from DeCelles, 2004). Black dots represent well log control points. (B and C) are maps showing the approximate locations of the paleoshoreline (red line) and distribution of sedimentary systems (indicated by formation/member names) at ca. 80 Ma (*Baculites asperiformis* zone) and ca. 77 Ma (*Baculites scotti* zone), respectively. Paleoshoreline locations are from Blakey (2014) and Cobban et al. (1994). The shape of the conjugate Shatsky Rise at ca. 80 Ma is outlined by blue dashed lines (from Humphreys et al., 2015). Maps B and C have exactly the same spatial extent as map A. KU—Kaibab uplift; MA—Moxa Arch; Sh.—Shale.

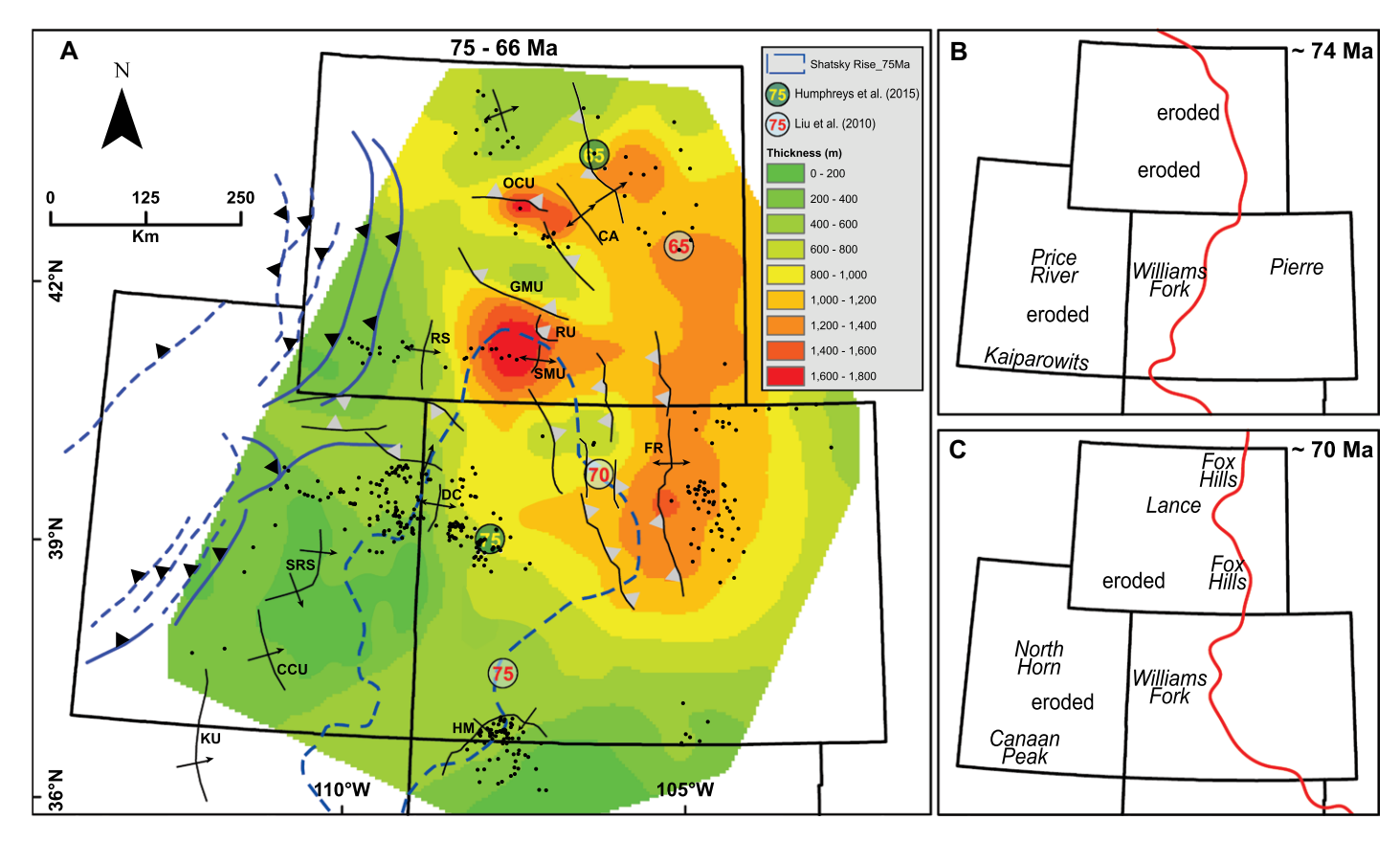


Figure 8. (A) Isopach map of late Campanian to Maastrichtian (ca. 75–66 Ma) strata in the study area. The moderate to high sedimentation rates in the area between the Piceance Basin and Denver Basin are probably artifacts (no control points in this area) based on projections of thickness trends from the eastern Piceance Basin and western Denver Basin. Solid and dashed barbed lines indicate active and inactive thrusts, respectively (from DeCelles, 2004). Black dots represent well log control points. (B and C) are maps showing the approximate locations of the paleoshoreline (red line) and distribution of sedimentary systems (indicated by formation/member names) at ca. 74 Ma (*Baculites compressus* zone) and ca. 70 Ma, respectively. Paleoshoreline locations are from Blakey (2014). The shape of the conjugate Shatsky Rise at ca. 75 Ma is outlined by blue dashed lines (from Humphreys et al., 2015). Maps B and C have exactly the same spatial extent as map A. CA—Casper arch; OCU—Owl Creek uplift; GMU—Granite Mountains uplift; RU—Rawlins uplift; SMU—Sierra Madre uplift; RS—Rock Springs uplift; DC—Douglas Creek arch; FR—Front Range; SRS—San Rafael Swell; CCU—Circle Cliffs uplift; KU—Kaibab uplift.

attributed to the long-wavelength dynamic subsidence in front of the conjugate Shatsky Rise. The increased subsidence rates (indicated by moderate to high sediment accumulation) in the northern Kaiparowits Plateau during this time interval is also noted in Roberts and Kirschbaum (1995) and Heller and Liu (2016). The coincidence in timing of the increased subsidence and Kaibab uplift suggests a possible causal relationship—flexural subsidence due to loading of the Kaibab uplift.

During the middle to late Campanian, southwestern Wyoming (Moxa Arch area) and central Utah were located at the presumed foredeep region in front of the thrust fronts and were expected to have large accommodation and record thick sediment accumulation when the sediment supply is high. The isopach map, however, indicates that southwestern Wyoming and central Utah are characterized by low sediment accumulation (Fig. 7), suggesting low rates of accommodation creation in these

areas, because sediment supply should not be a limiting factor at areas close to the thrust belt. The uplift of Moxa Arch resulted in erosion of several hundred meters of strata and a major unconformity at the base of the Trail Member of the Ericson Formation (Liu et al., 2005). The duration of this unconformity coincides with quiescence phase of Absaroka thrusts, indicating the uplift of Moxa Arch is associated with foredeep uplift/rebound (Liu et al., 2005). The low accommodation creation rates (indicated by low sediment accumulation) in central and eastern Utah, however, cannot be explained by foredeep rebound because thrusts in central Utah were active during this time (DeCelles, 2004). Instead, flexural subsidence generated by loading of the thrust sheets in central Utah probably interfered with dynamic uplift above the conjugate Shatsky Rise, resulting in the low accommodation areas in central and eastern Utah (Fig. 7).

4.4. Late Campanian to Maastrichtian (75–66 Ma) Deposition

Late Campanian to Maastrichtian strata record continued first-order regression of the seaway (Figs. 8B and 8C). The overall regression was interrupted by a short-term (2nd-order) marine transgression in the early late Maastrichtian (Kauffman, 1977). Rapid progradation of sedimentary systems with drainage of the basin followed as the WIS withdrew from the CFB by late Maastrichtian time.

Thrusting in the frontal Sevier belt continued in western Wyoming, central and southern Utah during the late Campanian to Maastrichtian (DeCelles, 2004). During 75–66 Ma, the conjugate Shatsky Rise continued to migrate northeastward from eastern-central Colorado to northeastern Wyoming (Fig. 8). Starting from the late Campanian, widespread Laramide intraforeland basement uplifts began to take place

within the CFB (Dickinson et al., 1988; Yonkee and Weil, 2015).

The isopach pattern of the late Campanian to Maastrichtian strata shows a more complex depocenter distribution within the CFB (Fig. 8). The isopach map reveals a broad depocenter (\sim 500 km \times 500 km) centered at \sim 300 km in front of the conjugate Shatsky Rise extending from central Colorado to eastern Wyoming. This broad depocenter, however, consists of at least four "sub-depocenters" (Wind River Basin, central Bighorn Basin, Washakie Basin, and western Denver Basin) with high sediment accumulation (>1000 m) separated by areas of low sediment accumulation (Fig. 8). Most areas, aside from this broad depocenter, show overall low sediment accumulation.

Interpretation

The development of depocenters within the CFB during the late Campanian to Maastrichtian can be largely attributed to the flexural subsidence due to lithospheric loading of adjacent Laramide-style uplifts. For instance, the elongated depocenter in western Denver Basin approximately follows the trend of the adjacent Front Range (Fig. 8). The thickness of late Campanian to Maastrichtian strata in the eastern Washakie Basin thins across the crestal areas of the Rock Springs, Granite Mountains, Rawlins, and Sierra Madre uplifts, indicating these structures were active during this time (Fig. 8). A more detailed stratigraphic analysis of the Canyon Creek Member of the Ericson Sandstone in southern Wyoming indicates the Rock Springs, Rawlins, and Sierra Madre uplifts were already active during the late Campanian (López and Steel, 2015; Fig. 8). The rapid southward thinning of late Campanian to Maastrichtian strata in the Wind River Basin indicates syn-depositional uplifts of the Casper Arch and Owl Creek uplift flanking the basin to the north (Fig. 8).

Minimal accommodation in southwestern Wyoming indicates this area was located at the wedge-top zone during the late Campanian to Maastrichtian, as a result of the eastward propagation of the thrust fronts (DeCelles, 2004). The broad low accommodation area in central, eastern, and southern Utah indicates accommodation generated by flexural loading (if any) of the Sevier thrust sheet was interfered by Laramide uplifts (e.g., San Rafael Swell, and Circle Cliffs uplift) or by effects of dynamic uplift above the migrating conjugate Shatsky Rise across this area. Local Laramide uplifts, however, are not likely to account for the low accommodation over such a broad area, especially lithospheric loading of these uplifts may result in high accommodation areas nearby (similar to these local subdepocenters in Wyoming). Therefore, the broad

low accommodation area in central and eastern Utah are probably produced due to the effects of dynamic uplift on the trailing part of the conjugate Shatsky Rise. For a similar reason, the broad depocenter extending from northcentral Colorado to eastern central Wyoming likely reflects some degrees of mantle-induced dynamic subsidence in front of the conjugate Shatsky Rise. The deviation from an expected broad area of dynamic subsidence (e.g., the broad depocenter in Fig. 7) is mainly due to overprinting by local uplift/subsidence induced by Laramide structures.

5. DISCUSSION

5.1. Isopach Patterns Representative of Flexural Subsidence versus Dynamic Subsidence

The observed isopach patterns, based on undecompacted isopach maps, are still considered to be reliable indicators of relative subsidence within the study area, especially on the regional scale and temporal scale that are focused in this study. Although the sediment accumulation (subsidence) rate of shale-rich successions may be underestimated based on undecompacted isopach maps, the highest rates of sediment accumulation occur mostly in shale-rich successions in all isopach maps (e.g., the primary depocenters in Figs. 5-6 and Figs. 7-8 consist dominantly of the Mancos Shale and Pierre Shale, respectively). In other words, the observed isopach patterns may still hold true (and may even be more distinct) when the effects of compaction have indeed been taken into account.

The 100-90 Ma and 80-75 Ma isopach maps can be considered as two end-members representing CFB developed under the dominant influence of flexural subsidence and dynamic subsidence, respectively. The 100-90 Ma isopach pattern shows well-developed foredeep, forebulge, and back-bulge depozones (Fig. 5), indicating accommodation within the CFB was mainly created by rapid flexural subsidence in response to loading of the Sevier thrust-and-fold belt. Although the preservation of forebulge deposits (northeastern Utah/northwestern Colorado in Fig. 5) can be used as evidence for dynamic subsidence that extends more than 1000 km inboard (DeCelles, 2012), no diagnostic feature of dynamic subsidence (i.e., long-wavelength, broad subsidence) is indicated by the 100-90 Ma isopach map. Instead, the well-developed and preservable forebulge deposits during this time probably reflect additional accommodation created at the forebulge by sea-level rise during the late Cenomanian/early Turonian global eustatic highstand. The depocenter distribution revealed by the 80-75 Ma isopach map, however, significantly departs from the well-organized flexural foreland basin geometry. During this time, the main depocenter within the CFB is much broader $(500 \text{ km} \times 500 \text{ km})$ and located > 500 km from the Sevier thrust front (Fig. 7). Flexural loading models cannot account for the anomalous subsidence pattern shown in Figure 7 without using unrealistically wide loads or an unrealistically rigid plate (Burgess and Moresi, 1999). By comparing with the reconstructed locations of the conjugate Shatsky Rise, the main depocenter ($>400 \text{ km} \times 400 \text{ km}$) within the CFB during 80–75 Ma was located \sim 500 km in front of the conjugate Shatsky Rise, where the magnitude of dynamic coupling is predicted to be the greatest (Mitrovica et al., 1989; Burgess and Moresi, 1999; Liu et al., 2010; Liu et al., 2011; Heller and Liu, 2016). Therefore, accommodation creation within the CFB was dominantly controlled by the downward sublithospheric mantle flow (downwelling) in front of the conjugate Shatsky Rise during 80-75 Ma. The transition from dominant flexural subsidence to dominant dynamic subsidence occurred at ca. 80 Ma in the CFB.

5.2. Fate of the Conjugate Shatsky Rise and Migration of Dynamic Topography

The approximate timing of the transition from dominant flexural subsidence to dominant dynamic subsidence within the CFB, based on new isopach maps developed in this study, is consistent with earlier studies investigating the subsidence mechanism of the CFB based on stratigraphic analysis (Roberts and Kirschbaum, 1995; Jones et al., 2011; Painter and Carrapa; 2013). Although the change in the dominant subsidence mechanism within the CFB has been generally attributed to the flat subduction of the conjugate Shatsky Rise (Jones et al., 2011; Painter and Carrapa, 2013), the effect of dynamic topography (including both uplift and subsidence) associated with the subduction of the oceanic plateau on the development of the CFB remains poorly constrained, largely due to scattered control points, general isopach patterns, and/or smaller study areas in earlier studies. In this study, the Late Cretaceous strata within the CFB was investigated over a much broader area based on denser well log control points (Fig. 2). By incorporating information on the timing and locations of Sevier-style and Laramide-style deformation and recent reconstruction (e.g., shape and path) of the conjugate Shatsky Rise (Liu et al., 2010; Humphreys et al., 2015), this study can therefore provide additional constraints on the role of dynamic topography associated with the subduction of the oceanic plateau in the development of CFB during the Late Cretaceous.

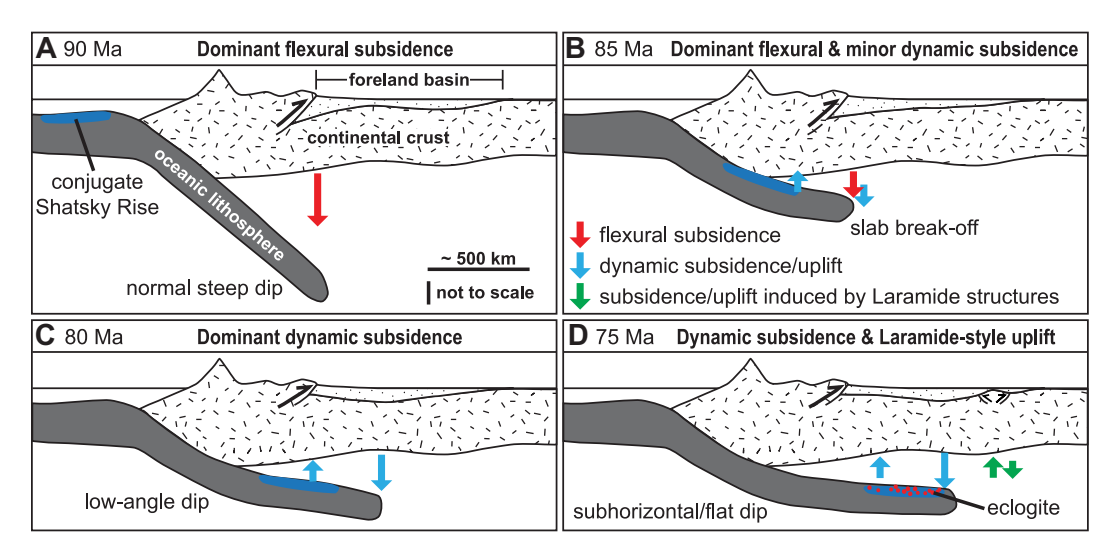


Figure 9. Schematic drawings showing the temporal change in effects of dynamic topography in response to the subduction of the conjugate Shatsky Rise (based on Aschoff and Steel. 2011; Humphreys et al., 2015; Liu and Currie, 2016; Axen et al., 2018; and results from this study). (A) At ca. 90 Ma, the conjugate Shatsky Rise collided with North America. The subduction of the Farallon plate had a normal dipping angle. The foreland basin had a well-developed flexural profile produced by the loading of the Sevier fold-and-thrust belt. (B)

A low-angle to flat segment of the Farallon plate beneath western North America started to form at ca. 85 Ma (Liu and Currie, 2016) due to the buoyant oceanic plateau crust. Dynamic subsidence started to influence the subsidence foreland basin, particularly at areas in front of the conjugate Shatsky Rise, making the flexural foreland basin geometry more subdued. (C) Dynamic subsidence became the dominant subsidence mechanism at ca. 80 Ma. The conjugate Shatsky Rise remained relatively buoyant, and dynamic subsidence is predicted to be the greatest at its front. (D) The conjugate Shatsky Rise was starting to lose its buoyancy by transforming into eclogite at ca. 75 Ma (Humphreys et al., 2015). The greatest dynamic subsidence occurs directly in front of, or even above, the leading part of the conjugate Shatsky Rise.

Geological reconstructions and seismic tomography indicate that an oceanic plateau, the conjugate Shatsky Rise, was subducted below southern California starting at ca. 90 Ma (Liu et al., 2010; Humphreys et al., 2015). The initially buoyant oceanic plateau crust (basaltic in composition), as well as its underlying lowdensity depleted mantle layer, have led to the formation of a low-angle to flat segment of the Farallon plate beneath western North America starting at ca. 85 Ma (Fig. 9B; Liu and Currie, 2016). The magnitude of dynamic subsidence is predicted to be the greatest in areas above the front of the conjugate Shatsky Rise because, first, the more steeply dipping slab in front of the flat slab would enhance dynamic coupling (downwelling) between the Farallon and North American plates, increasing dynamic subsidence (Heller and Liu, 2016). Second, the frontal Farallon slab probably has larger negative buoyancy because it is older in age and may have undergone eclogitization (Liu et al., 2010). In contrast, areas above the conjugate Shatsky Rise would experience isostatic uplift (or much decreased dynamic subsidence) due to the overall buoyant oceanic plateau. Therefore, changes in the dynamic topography within the Late Cretaceous CFB revealed by the newly developed isopach maps can provide additional constraints on the fate of the conjugate Shatsky Rise through the Late Cretaceous.

The earliest influence of dynamic topography on the development of CFB appears to have been recorded in the 90–80 Ma isopach map (Fig. 6). The moderate accommodation at

the four corners region was likely created due to long-wavelength dynamic subsidence in front of the conjugate Shatsky Rise (see Fig. 1 for the approximate location of conjugate Shatsky Rise at ca. 85 Ma). The low accommodation in southern Utah is probably related to decreased dynamic subsidence (or isostatic uplift) above the conjugate Shatsky Rise, which has presumably migrated to beneath northern Arizona by 80 Ma (Fig. 6; Humphreys et al., 2015). Despite the general agreement on the location of the conjugate Shatsky Rise at 85 Ma (Fig. 1), the isopach pattern shown in Figure 6 (i.e., relatively low and high accommodation at southern Utah and the four corners region, respectively) is more consistent with the predicted position of dynamic topography produced by the conjugate Shatsky Rise if it were located beneath northern Arizona at 80 Ma as indicated by Humphreys et al. (2015).

During 80–75 Ma, the conjugate Shatsky Rise passed beneath the Colorado Plateau (Fig. 1). The relatively low accommodation (indicated by low sediment accumulation) in areas above the path of the conjugate Shatsky Rise (Fig. 7), as well as uplift of the southwestern Colorado Plateau (Flowers et al., 2008) during this time, indicates conjugate Shatsky Rise remained relatively buoyant (having a basaltic crust). The broad depocenter (>400 km \times 400 km) shown in the 80–75 isopach map lies $\sim\!500$ km directly in front of the conjugate Shatsky Rise (Figs. 7 and 9C). The elongation orientation of the broad depocenter should probably be parallel to the migration direc-

tion of the conjugate Shatsky Rise (because dynamic subsidence is predicted to be the greatest at its front), indicating the location of the conjugate Shatsky Rise at 75 Ma is located somewhere in between its proposed locations at 75 Ma by Liu et al. (2010) and Humphreys et al. (2015) (Fig. 7).

From 75 to 66 Ma, the migration path of the conjugate Shatsky Rise shows a more northward deflection (Fig. 8). Assuming the depocenter generated by dynamic subsidence also migrated in the same direction, a high accommodation area is expected in eastern or northeastern Wyoming, which appears to be consistent with the isopach pattern in Figure 8. The segregated depocenter distribution revealed by Figure 8, however, indicates flexural subsidence caused by local Laramide uplifts significantly overprinted the typically broad pattern of dynamic subsidence/uplift. For instance, the thickness trend of the 75-66 Ma strata in the Washakie Basin and Wind River Basin indicates surrounding Laramide uplifts were active nearby (Fig. 8). Nevertheless, the accommodation created in the Washakie Basin and Wind River Basin is almost as large in magnitude as the accommodation created by loading of the Sevier thrust sheets in central Utah during 90-80 Ma (Fig. 6). This indicates part of the accommodation in these local Laramide basins was created by dynamic subsidence related to subduction of the conjugate Shatsky Rise (Fig. 8). The wavelength of dynamic subsidence, however, seems to have significantly decreased during 75-66 Ma (~250 km in

front of the conjugate Shatsky Rise) comparing to the 80-75 Ma isopach map. The greatest dynamic subsidence occurs directly in front of, or even above, the leading part of the conjugate Shatsky Rise starting at 75 Ma. The decrease in the dynamic subsidence wavelength indicates that the conjugate Shatsky Rise was starting to lose its buoyancy by transforming into eclogite at ca. 75 Ma (the leading part of the conjugate Shatsky Rise would undergo eclogitization first). As the eclogitized oceanic plateau migrated farther inboard and subducted into deeper depth, the magnitude and wavelength of dynamic subsidence would have decreased because there would have been less coupling between the Farallon and North American plates (Fig. 9D). At ca. 70 Ma, the conjugate Shatsky Rise was approximately located beneath the broad depocenter shown in Figure 8, indicating that all the basalt crust of the conjugate Shatsky Rise may have transformed into eclogite by 70 Ma. The emplacement of the antibuoyant conjugate Shatsky Rise starting at 70 Ma would have caused subsidence directly above it, as shown in the isopach pattern (Fig. 8). The timing of eclogitization of the conjugate Shatsky Rise indicated by isopach analysis is consistent with numerical modeling results (Liu et al., 2010) and other geologic evidence (e.g., the initiation of Colorado Mineral Belt at 75 Ma; Humphreys et al., 2015).

5.3. Transitory Effects of Dynamic Topography: Implications for Geodynamic Modeling of Dynamic Subsidence

Most current geodynamic models of dynamic subsidence are static in the sense that they only consider effects of dynamic subsidence under steady conditions with a limited number of variables. Results from this study, however, indicate the effects of dynamic topography (e.g., wavelength and location of subsidence and uplift) generated in response to the subduction of an oceanic plateau are rather transitory. Dynamic topography started to influence creation/destruction of accommodation in the CFB from ca. 85 Ma, became the dominant subsidence mechanism at ca. 80 Ma, and was significantly overprinted by the flexural subsidence induced by local Laramide uplift and loading during 75-66 Ma. Although the influence of dynamic subsidence in the CFB has been generally inferred based on the unexplainable amount of subsidence when loading from orogenic belts and sediments are taken into account, the new isopach maps with higher spatial resolution developed herein indicate the effects of dynamic topography are highly variable through both space

and time, largely controlled by the evolution of the conjugate Shatsky Rise. For instance, the area of dynamic subsidence within the CFB, as revealed in the 90-80 Ma and 80-75 Ma isopach maps, seemed to have migrated from the four corners region at 85 Ma (Fig. 6) to north-central Colorado at 80 Ma (Fig. 7), at an average rate of \sim 120 km/ m.y. The area of dynamic subsidence subsequently migrated from north-central Colorado at 80 Ma (Fig. 7) to southeastern/eastern Wyoming at 75 Ma (Fig. 8), at an average rate of 60 km/m.y. Additionally, based on the comparison between the 80-75 Ma and 75-66 Ma isopach maps, the wavelength of dynamic subsidence greatly decreased from \sim 500 km (Fig. 7) to \sim 300 km (Fig. 8). The decreases in the migration rate and wavelength of dynamic subsidence can be largely attributed to the loss of buoyancy of the conjugate Shatsky Rise, as the oceanic plateau had subducted to deeper depth and undergone eclogitization (Section 5.2; Figs. 9C and 9D). Therefore, changes in the location, subduction angle, and depth, and buoyancy of the subducting oceanic plateau through the Late Cretaceous may lead to changes in the wavelength and locations of dynamic subsidence and uplift within the CFB. The transitory effects of mantle-induced dynamic topography need to be taken into account in future geodynamic models to better reconstruct and predict the development of other retroarc foreland basins.

6. CONCLUSIONS

New isopach maps developed in this study, based on the stratigraphic correlation of Late Cretaceous strata over a broader area in the western United States with stronger temporal constraints and denser well log control points, provide additional constraints on the effects of dynamic topography on the development of Late Cretaceous Cordilleran foreland basin (CFB) and the fate of the conjugate Shatsky Rise. The main conclusions are as follows:

- (1) Dynamic topography may have started to influence the development of the CFB as early as 85 Ma, despite that flexural subsidence was the dominant mechanism controlling subsidence of CFB during ca. 100–80 Ma. The 100–90 Ma isopach map shows well-developed foredeep, forebulge, and backbulge. The well-organized flexural foreland basin geometry, however, becomes more subdued in the 90–80 Ma isopach map, probably reflecting the interference between flexural subsidence with mantle-driven dynamic subsidence.
- (2) Long-wavelength subsidence is the most diagnostic feature of dynamic subsidence. Based on temporal changes in depocenter distribu-

tions, dynamic subsidence is inferred to influence accommodation creation in the CFB starting from ca. 85 Ma and became the dominant subsidence mechanism in CFB at ca. 80 Ma. The effects of dynamic subsidence changed significantly in character when the conjugate Shatsky Rise began to lose its buoyancy during 75–70 Ma. Subsidence within the CFB during 75–66 Ma was controlled by the combined effects of dynamic subsidence and flexural subsidence induced by local Laramide uplifts.

- (3) Large-scale (>400 km \times 400 km) dynamic topography (subsidence and uplift) significantly influenced the depocenter development within the CFB, which is most distinctly revealed in the 80–75 Ma isopach map. Preliminary isopach maps of successive time intervals suggest dynamic topography migrated at an average rate ranging from \sim 120 km to 60 km/m.y. in the CFB through the Late Cretaceous. The size and migration rate of dynamic topography can be further constrained in future studies with more control points and higher-resolution stratigraphic correlations.
- (4) Dynamic topography generated in response to the subduction of an oceanic plateau is rather transitory. The effects of dynamic topography (e.g., wavelength and locations of subsidence and uplift, migration rate) on the development of CFB varied through both space and time in response to the evolution of conjugate Shatsky Rise (e.g., changes in location, subduction angle and depth, buoyancy through time). Careful reconstruction of regional geologic history based on stratigraphic analysis using three-dimensional data sets is required to constrain the influence of dynamic topography in other retroarc foreland basins. A better understanding of how transitory effects of dynamic topography may vary through both space and time is critical for future geodynamic models to better reconstruct and predict the development of other foreland basins that may have formed by an interplay of crustal and asthenospheric tectonic processes.

ACKNOWLEDGMENTS

We are grateful for the constructive review and editorial comments of Science Editor Dr. Rob Strachan, Associate Editor Dr. Michael Smith, and two anonymous reviewers. This research was partially supported by National Science Foundation grant EAR-1824550. Additionally, we wish to thank a host of graduate students at Colorado School of Mines and the University of Alaska Anchorage who contributed much of the stratigraphic groundwork and data used in the regional database: Nick Daniele, Sarah Edwards, Jared Rountree, Brock Rust, Raju Sitaula, Parker Valora, and Michelle Wiechman.

REFERENCES CITED

Anna, L.O., 2012, West-east lithostratigraphic cross section of Cretaceous rocks from central Utah to western

- Kansas: U.S. Geological Survey Open-File Report 2012-1074, 2 p., https://doi.org/10.3133/ofr20121074.
- Antia, J., and Fielding, C.R., 2011, Sequence stratigraphy of a condensed low-accommodation succession: Lower Upper Cretaceous Dakota Sandstone, Henry Mountains, southeastern Utah: AAPG Bulletin, v. 95, p. 413–447, https://doi.org/10.1306/06301009182.
- Aschoff, J.L., 2008, Controls on the development of clastic wedges and growth strata in foreland basins: Examples from Cretaceous Cordilleran foreland basin strata, USA [Ph.D. thesis]: Austin, Texas, USA, The University of Texas at Austin, 199 p.
- Aschoff, J.L., 2014, The importance of stratigraphic architecture in tracking the migration of dynamic subsidence in the Cordilleran Foreland Basin: Geological Society of America Abstracts with Programs, v. 46, no. 6, p. 586.
- Aschoff, J., and Steel, R., 2011, Anomalous clastic wedge development during the Sevier-Laramide transition, North American Cordilleran foreland basin, USA: Geological Society of America Bulletin, v. 123, p. 1822–1835, https://doi.org/10.1130/B30248.1
- Axen, G.J., van Wijk, J.W., and Currie, C.A., 2018, Basal continental mantle lithosphere displaced by flat-slab subduction: Nature Geoscience, v. 11, p. 961–964, https://doi.org/10.1038/s41561-018-0263-9.
- Blakey, R.C., 2014, Paleogeography and Paleotectonics of the Western Interior Seaway, Jurassic-Cretaceous of North America: AAPG Search and Discovery Article #30392, p. 1–72.
- Burgess, P.M., and Moresi, L., 1999, Modelling rates and distribution of subsidence due to dynamic topography over subducting slabs: Is it possible to identify dynamic topography from ancient strata?: Basin Research, v. 11, p. 305–314, https://doi.org/10.1046/ j.1365-2117.1999.00102.x.
- Bush, M.A., Horton, B.K., Murphy, M.A., and Stockli, D.F., 2016, Detrital record of initial basement exhumation along the Laramide deformation front, southern Rocky Mountains: Tectonics, v. 35, p. 2117–2130, https://doi .org/10.1002/2016TC004194.
- Catuneanu, O., 2019, Model-independent sequence stratigraphy: Earth-Science Reviews, v. 188, p. 312–388, https://doi.org/10.1016/j.earscirev.2018.09.017.
- Catuneanu, O., Beaumont, C., and Waschbusch, P., 1997, Interplay of static loads and subduction dynamics in foreland basins: Reciprocal stratigraphies and the "missing" peripheral bulge: Geology, v. 25, p. 1087–1090, https://doi.org/10.1130/0091-7613(1997)025<1087:IO SLAS>2.3.CO;2.
- Chamberlain, V.E., Lambert, R.S.J., and McKerrow, W.S., 1989, Mesozoic sedimentation rates in the Western Canada Basin as indicators of the time and place of tectonic activity: Basin Research, v. 2, p. 189–202, https:// doi.org/10.1111/j.1365-2117.1989.tb00034.x.
- Cobban, W.A., Walaszczyk, I., Obradovich, J.D., and McKinney, K.C., 2006, A USGS zonal table for the Upper Cretaceous middle Cenomanian–Maastrichtian of the Western Interior of the United States based on ammonites, inoceramids, and radiometric ages: U.S. Geological Survey Open-File Report 2006-1250, 46 p., https:// doi.org/10.3133/ofr20061250.
- Cobban, W.A., Merewether, E.A., Fouch, T.D., and Obradovich, J.D., 1994, Some Cretaceous shorelines in the western interior of the United States, in Caputo, M.V., Peterson, J.A., Franczyk, K.J., eds., Mesozoic systems of the Rocky Mountain region, USA: Denver, Colorado, Rocky Mountain Section SEPM, p. 393–414.
- Connor, C.W., 1992, The Lance Formation: Petrography and stratigraphy, Powder River basin and nearby basins, Wyoming and Montana, in Evolution of Sedimentary Basins: Powder River Basin: U.S. Geological Survey Bulletin Series 1917-I, 17 p., https://doi.org/10.3133/ b1917I.
- Corbett, M.J., Fielding, C.R., and Birgenheier, L.P., 2011, Stratigraphy of a Cretaceous coastal-plain fluvial succession: The Campanian Masuk Formation, Henry Mountains syncline, Utah, U.S.A: Journal of Sedimentary Research, v. 81, p. 80–96, https://doi.org/10.2110/ jsr.2011.12.
- Daniele, N.P., 2012, Reservoir characterization and stratigraphic distribution of "tight" gas sandstones of the Upper Mesaverde Group, Uinta Basin, Utah: Implications

- for predicting better gas production [M.S. thesis]: Golden, Colorado, USA, Colorado School of Mines, 164 p.
- DeCelles, P.G., 2004, Late Jurassic to Eocene evolution of the Cordilleran thrust belt and foreland basin system, western U.S.A: American Journal of Science, v. 304, p. 105–168, https://doi.org/10.2475/ajs.304.2.105.
- DeCelles, P.G., 2012, Foreland basin systems revisited: Variations in response to tectonic settings, in Busby, C., and Azor, A., eds., Tectonics of Sedimentary Basins, p. 405–426, https://doi.org/10.1002/9781444347166.ch20.
- DeCelles, P.G., and Giles, K.A., 1996, Foreland basin systems: Basin Research, v. 8, p. 105–123, https://doi.org/10.1046/j.1365-2117.1996.01491.x.
- Dickinson, W.R., Klute, M.A., Hayes, M.J., Janecke, S.U., Lundin, E.R., McKittrick, M.A., and Olivares, M.D., 1988, Paleogeographic and paleotectonic setting of Laramide sedimentary basins in the central Rocky Mountain region: Geological Society of America Bulletin, v. 100, p. 1023–1039, https://doi.org/10.1130/0016-7606(1988)100<1023:PAPSOL>2.3.CO;2.
- Edwards, S.A., 2011, Outcrop-to-subsurface sequencestratigraphic framework of the Rollins Sandstone of the lles Formation and Lower Williams Fork Formation: Implications for predicting "sweet-spots" in tight-gassandstone reservoirs, Piceance Basin, Colorado [M.S. thesis]: Golden, Colorado, USA, Colorado School of Mines, 179 p.
- Elder, W.P., and Kirkland, J.I., 1994, Cretaceous paleogeography of the southern Western Interior region, in Caputo, M.V., Peterson, J.A., and Franczyk, K.J., eds., Mesozoic Systems of the Rocky Mountain Region, USA: SEPM (Society for Sedimentary Geology), Rocky Mountain Section, p. 415–440.
- Fassett, J.E., 2010, Oil and gas resources of the San Juan Basin, New Mexico and Colorado, in Fassett, J.E., Zeigler, K.E., and Lueth, V., eds., Geology of the Four Corners Country: New Mexico Geological Society, 61st Annual Fall Field Conference Guidebook, p. 181–196.
- Finn, T.M., 2007, Subsurface stratigraphic cross sections of Cretaceous and lower Tertiary rocks in the Wind River Basin, central Wyoming, in U.S. Geological Survey Wind River Basin Assessment Team, eds., Petroleum Systems and Geologic Assessment of Oil and Gas Resources in the Wind River Basin Province, Wyoming: U.S. Geological Survey Data Series 69-J-9, 32 p., https://doi.org/10.3133/ds69J9.
- Finn, T.M., 2010, Subsurface stratigraphic cross sections showing correlation of Cretaceous and Lower Tertiary Rocks in the Bighorn Basin, Wyoming and Montana, in U.S. Geological Survey Bighorn Basin Province Assessment Team, eds., Petroleum Systems and Geologic Assessment of Oil and Gas in the Bighorn Basin Province, Wyoming and Montana: U.S. Geological Survey Digital Data Series DDS-69-V, 17 p.
- Finn, T.M., and Johnson, R.C., 2005, Subsurface stratigraphic cross sections of Cretaceous and lower Tertiary rocks in the Southwestern Wyoming Province, Wyoming, Colorado, and Utah, in USGS Southwestern Wyoming Province Assessment Team, eds., Petroleum Systems and Geologic Assessment of Oil and Gas in the Southwestern Wyoming Province, Wyoming, Colorado, and Utah: U.S. Geological Survey Digital Data Series DDS-69-D, 15 p.
- Flament, N., Gurnis, M., and Müller, R.D., 2013, A review of observations and models of dynamic topography: Lithosphere, v. 5, p. 189–210, https://doi.org/10.1130/L245.1.
- Flowers, R.M., Wernicke, B.P., and Farley, K.A., 2008, Unroofing, incision, and uplift history of the southwestern Colorado Plateau from apatite (U-Th)/He thermochronometry: Geological Society of America Bulletin, v. 120, p. 571–587, https://doi.org/10.1130/ B26231.1.
- Fouch, T.D., Lawton, T.F., Nichols, D.J., Cashion, W.B., and Cobban, W.A., 1983, Patterns and timing of synorogenic sedimentation in Upper Cretaceous rocks of central and northeast Utah, in Reynolds, M.W., and Dolly, E.D., eds., Mesozoic Paleogeography of the West-Central United States: Proceedings of the 2nd Rocky Mountain Paleogeography Symposium, Denver, Colorado, USA, Society of Economic Paleontologists and Mineralogists, Rocky Mountain Section, p. 305–336.

- Franczyk, K.J., Pitman, J.K., and Nichols, D.J., 1990, Sedimentology, mineralogy, palynology, and depositional history of some uppermost Cretaceous and lowermost Tertiary rocks along the Utah Book and Roan cliffs east of the Green River: U.S. Geological Survey Bulletin Series 1787-N, 27 p., https://doi.org/10.3133/b1787N.
- Gill, J.R., Cobban, W.A., and Schultz, L.G., 1972, Stratig-raphy and composition of the Sharon Springs Member of the Pierre Shale in western Kansas: U.S. Geological Survey Professional Paper 728, 50 p., https://doi.org/10.3133/pp728.
- Gradstein, F.M., Ogg, J.G., Schmitz, M.D., and Ogg, G.M., 2012. The Geologic Time Scale 2012: Amsterdam, The Netherlands, Elsevier, 1176 p.
- Gurnis, M., 1992, Rapid continental subsidence following the initiation and evolution of subduction: Science, v. 255, p. 1556–1558, https://doi.org/10.1126/ science.255.5051.1556.
- Hampson, G.J., Davies, W., Davies, S.J., Howell, J.A., and Adamson, K.R., 2005, Use of spectral gamma-ray data to refine subsurface fluvial stratigraphy: Late Cretaceous strata in the Book Cliffs, Utah, USA: Journal of the Geological Society, v. 162, p. 603–621, https://doi .org/10.1144/0016-764904-059.
- Heller, P.L., and Liu, L., 2016, Dynamic topography and vertical motion of the U.S. Rocky Mountain region prior to and during the Laramide orogeny: Geological Society of America Bulletin, v. 128, p. 973–988, https://doi.org/10.1130/B31431.1.
- Hettinger, R.D., Roberts, L.N.R., Biewick, L.R.H., and Kirschbaum, M.A., 2000, Geologic overview and resource assessment of coal in the Kaiparowits Plateau, southern Utah: U.S. Geological Survey Professional Paper 1625-B, 69 p.
- Higley, D.K., and Cox, D.O., 2007, Oil and gas exploration and development along the front range in the Denver basin of Colorado, Nebraska, and Wyoming, in Higley, D.K., ed., Petroleum Systems and Assessment of Undiscovered Oil and Gas in the Denver Basin Province, Colorado, Kansas, Nebraska, South Dakota, and Wyoming—USGS Province 39: U.S. Geological Survey Digital Data Series DDS-69-P, 45 p.
- Higley, D.K., and Schmoker, J.W., 1989, Influence of depositional environment and diagenesis on regional porosity trends in the Lower Cretaceous J sandstone, Denver basin, Colorado, in Coalson, E.B., ed., Petrogenesis and Petrophysics of Selected Sandstone Reservoirs of the Rocky Mountain Region: Denver, Colorado, USA, Rocky Mountain Association of Geologists, p. 183–196.
- Humphreys, E.D., Schmandt, B., Bezada, M.J., and Perry-Houts, J., 2015, Recent craton growth by slab stacking beneath Wyoming: Earth and Planetary Science Letters, v. 429, p. 170–180, https://doi.org/10.1016/j.epsl.2015.07.066.
- Izett, G.A., Cobban, W.A., and Gill, J.R., 1971, The Pierre Shale near Kremmling, Colorado, and its correlation to the east and the west: U.S. Geological Survey Professional Paper 684-A, 18 p., https://doi.org/10.3133/ pp684A.
- Jervey, M.T., 1988, Quantitative geological modeling of siliciclastic rock sequences and their seismic expression, in Wilgus, C.K., Hastings, B.S., Posamentier, H., Van Wagoner, J., Ross, C.A., and Kendall, C.G.S.C., eds., Sea-Level Changes: An Integrated Approach: Society of Economic Paleontologists and Mineralogists, p. 47–69, https://doi.org/10.2110/pec.88.01.0047.
- Jinnah, Z.A., and Roberts, E.M., 2011, Facies associations, paleoenvironment, and base-level changes in the Upper Cretaceous Wahweap Formation, Utah, U.S.A: Journal of Sedimentary Research, v. 81, p. 266–283, https://doi. org/10.2110/jsr.2011.22
- Jones, C.H., Farmer, G.L., Sageman, B., and Zhong, S., 2011, Hydrodynamic mechanism for the Laramide orogeny: Geosphere, v. 7, p. 183–201, https://doi.org/10.1130/ GES00575.1.
- Joo, Y.J., and Sageman, B.B., 2014, Cenomanian To Campanian carbon isotope chemostratigraphy from the Western Interior Basin, U.S.A: Journal of Sedimentary Research, v. 84, p. 529–542, https://doi.org/10.2110/ jsr.2014.38.

- Jordan, T.E., 1981, Thrust loads and foreland basin evolution, Cretaceous, western United States: AAPG Bulletin, v. 65, p. 2506–2520.
- Kauffman, E.G., 1977, Geological and biological overview: Western Interior Cretaceous basin: The Mountain Geologist, v. 14, p. 75–99.
- Kauffman, E.G., 1985, Cretaceous evolution of the Western Interior Basin of the United States, in Pratt, L.M., Kauffman, E.G., and Zelt, F.B., eds., Fine-grained Deposits and Biofacies of the Cretaceous Western Interior Seaway: Evidence of Cyclic Sedimentary Processes: Society of Economic Paleontologists and Mineralogists, 1985 Midyear Meeting, Golden, Colorado, USA, Field Trip Guidebook 4, p. iv–xiii.
- Kirschbaum, M.A., and Hettinger, R.D., 2004, Facies analysis and sequence stratigraphic framework of upper Campanian strata (Neslen and Mount Garfield formations, Bluecastle Tongue of the Castlegate sandstone, and Mancos shale), Eastern Book cliffs, Colorado and Utah: U.S. Geological Survey Data Series DDS-69-G, 46 p., https://doi.org/10.3133/ds69G.
- Kirschbaum, M.A., and Mercier, T.J., 2013, Controls on the deposition and preservation of the Cretaceous Mowry Shale and Frontier Formation and equivalents, Rocky Mountain region, Colorado, Utah, and Wyoming: AAPG Bulletin, v. 97, p. 899–921, https://doi .org/10.1306/10011212090.
- Laskowski, A.K., DeCelles, P.G., and Gehrels, G.E., 2013, Detrital zircon geochronology of Cordilleran retroarc foreland basin strata, western North America: Tectonics, v. 32, p. 1027–1048, https://doi.org/10.1002/ tect.20065.
- Lawton, T.F., 1986, Fluvial systems of the Upper Cretaceous Mesaverde Group and Paleocene North Horn Formation, central Utah: A record of transition from thin-skinned to thick-skinned deformation in the foreland region, in Peterson, J.A., ed., Paleotectonics and Sedimentation in the Rocky Mountain Region, United States: AAPG Memoir 41, p. 423–442, https://doi.org/10.1306/M41456C20.
- Lawton, T.F., 2008, Laramide Sedimentary Basins, in Miall, A.D., ed., The Sedimentary Basins of the United States and Canada, in Hsü, K.J., ed., Sedimentary Basins of the World: Amsterdam, The Netherlands, Elsevier, v. 5, p. 429–450.
- Lawton, T.F., and Bradford, B.A., 2011, Correlation and provenance of Upper Cretaceous (Campanian) fluvial strata, Utah, U.S.A., from zircon U-Pb geochronology and petrography: Journal of Sedimentary Research, v. 81, p. 495–512, https://doi.org/10.2110/jsr.2011.45.
- Lawton, T.F., Schellenbach, W.L., and Nugent, A.E., 2014, Late Cretaceous fluvial-megafan and axial-river systems in the southern Cordilleran foreland basin: Drip Tank Member of Straight Cliffs Formation and adjacent strata, southern Utah, U.S.A: Journal of Sedimentary Research, v. 84, p. 407–434, https://doi.org/10.2110/ jsr.2014.33.
- López, J.L., and Steel, R.J., 2015, Laramide signals and architecture of a widespread fluvial sand Sheet: Canyon Creek Member, southern Wyoming, U.S.A: Journal of Sedimentary Research, v. 85, p. 1102–1122, https://doi .org/10.2110/jsr.2015.67.
- Liu, L., Spasojević, S., and Gurnis, M., 2008, Reconstructing Farallon plate subduction beneath North America back to the Late Cretaceous: Science, v. 322, p. 934–938, https://doi.org/10.1126/science.1162921.
- Liu, L., Gurnis, M., Seton, M., Saleeby, J., Müller, R.D., and Jackson, J.M., 2010, The role of oceanic plateau subduction in the Laramide orogeny: Nature Geoscience, v. 3, p. 353–357, https://doi.org/10.1038/ ngeo829.
- Liu, S., and Currie, C.A., 2016, Farallon plate dynamics prior to the Laramide orogeny: Numerical models of flat subduction: Tectonophysics, v. 666, p. 33–47, https://doi .org/10.1016/j.tecto.2015.10.010.
- Liu, S., Nummedal, D., Yin, P., and Luo, H., 2005, Linkage of Sevier thrusting episodes and Late Cretaceous foreland basin megasequences across southern Wyoming (USA): Basin Research, v. 17, p. 487–506, https://doi .org/10.1111/j.1365-2117.2005.00277.x.
- Liu, S., Nummedal, D., and Liu, L., 2011, Migration of dynamic subsidence across the Late Cretaceous United States Western Interior Basin in response to Farallon

- plate subduction: Geology, v. 39, p. 555–558, https://doi.org/10.1130/G31692.1.
- Liu, S., Nummedal, D., and Gurnis, M., 2014, Dynamic versus flexural controls of Late Cretaceous Western Interior Basin, USA: Earth and Planetary Science Letters, v. 389, p. 221–229, https://doi.org/10.1016/ j.epsl.2014.01.006.
- Livaccari, R.F., 1991, Role of crustal thickening and extensional collapse in the tectonic evolution of the Sevier-Laramide orogeny, western United States: Geology, v. 19, p. 1104–1107, https://doi.org/10.1130/0091-7613(1991)019<1104:ROCTAE>2.3.CO:2.
- Luo, H., and Nummedal, D., 2012, Forebulge migration: A three-dimensional flexural numerical modeling and subsurface study of southwestern Wyoming, in Gao, D., ed., Tectonics and Sedimentation: Implications for Petroleum Systems: AAPG Memoir 100, p. 377–395.
- Lynds, R.M., and Slattery, J.S., 2017, Correlation of the Upper Cretaceous strata of Wyoming: Wyoming State Geological Survey Open File Report 2017-3.
- McGookey, D.P., Haun, J.D., Hale, L.A., Goodell, H.G., McCubbin, D.G., Weimer, R.J., and Wulf, G.R., 1972, Cretaceous system, in Mallory, W.W., ed., Geologic Atlas of the Rocky Mountain Region: Denver, Colorado, USA, Rocky Mountain Association of Geologists, p. 190–228.
- Merewether, E.A., 1996, Stratigraphy and tectonic implications of Upper Cretaceous rocks in the Powder River basin, northeastern Wyoming and southeastern Montana: U.S. Geological Survey Bulletin 1917-T, 92 p., https://doi.org/10.3133/b1917 T.
- Merewether, E.A., Cobban, W.A., and Obradovich, J.D., 2011, Biostratigraphic data from Upper Cretaceous formations-eastern Wyoming, central Colorado, and northeastern New Mexico: U.S. Geological Survey Scientific Investigations Map 3175, 10 p.
- Mitchum, R.M., and Van Wagoner, J.C., 1991, High-frequency sequences and their stacking patterns: Sequence-stratigraphic evidence of high-frequency eustatic cycles: Sedimentary Geology, v. 70, p. 131–160, https://doi.org/10.1016/0037-0738(91)90139-5.
- Mitrovica, J.X., Beaumont, C., and Jarvis, G.T., 1989, Tilting of continental interiors by the dynamical effects of subduction: Tectonics, v. 8, p. 1079–1094, https://doi .org/10.1029/TC008i005p01079.
- Molenaar, C.M., and Baird, J.K., 1989, North-south stratigraphic cross sections of upper Cretaceous rocks, northern San Juan Basin, southwestern Colorado: U.S. Geological Survey Miscellaneous Field Studies Map 2068, https://doi.org/10.3133/mf2068.
- Molenaar, C.M., and Cobban, W.A., 1991, Middle Cretaceous stratigraphy on the south and east sides of the Uinta Basin, northeastern Utah and northwestern Colorado, in Evolution of Sedimentary Basins: Uinta and Piceance Basins: U.S. Geological Survey Bulletin 1787-P, 34 p., https://doi.org/10.3133/b1787P.
- Molenaar, C.M., Cobban, W.A., Merewether, E.A., Pillmore, C.L., Wolfe, D.G., and Holbrook, J.M., 2002, Regional stratigraphic cross sections of Cretaceous rocks from east-central Arizona to the Oklahoma Panhandle: U.S. Geological Survey Miscellaneous Field Studies Map 2382, https://doi.org/10.3133/mf2382.
- Mulhern, J.S., and Johnson, C.L., 2017, Time-space variability of paralic strata deposited in a high accommodation, high sediment supply setting: Example from the Cretaceous of Utah, in Hampson, G.J., Reynolds, A.D., Kostic, B., and Wells, M.R., eds., Sedimentology of Paralic Reservoirs: Recent Advances: Geological Society of London, Special Publications, v. 444, p. 349–392, https://doi.org/10.1144/SP444.7.
- Ogg, J.G., Hinnov, L.A., and Huang, C., 2012, Cretaceous, in Gradstein, F.M., Ogg, J.G., Schmitz, M.D., and Ogg, G.M., eds., The Geologic Time Scale: Boston, Massachusetts, USA, Elsevier, p. 793–853, https://doi .org/10.1016/B978-0-444-59425-9.00027-5.
- Painter, C.S., and Carrapa, B., 2013, Flexural versus dynamic processes of subsidence in the North American Cordillera foreland basin: Geophysical Research Letters, v. 40, p. 4249–4253, https://doi.org/10.1002/ orl 50831
- Pang, M., and Nummedal, D., 1995, Flexural subsidence and basement tectonics of the Cretaceous Western Interior basin, United States: Geology, v. 23, p. 173–176,

- https://doi.org/10.1130/0091-7613(1995)023<0173:FS ABTO>2.3.CO;2.
- Patterson, P., Kronmueller, K., and Davies, T., 2003, Sequence stratigraphy of the Mesaverde group and Ohio Creek conglomerate, northern Piceance basin, Colorado, in Peterson, K.M., Olson, T.M., and Anderson, D.S., eds., Piceance Basin 2003 Guidebook: Denver, Colorado, USA, Rocky Mountain Association of Geologists, p. 115–128.
- Posamentier, H.W., Jervey, M.T., and Vail, P.R., 1988, Eustatic controls on clastic deposition I—Conceptual frameworks, in Wilgus, C.K., Hastings, B.S., Kendall, C.G.S.C., Posamentier, H.W., Ross, C.A., and Van Wagoner, J.C., eds., Sea-Level Changes: An Integrated Approach: Society of Economic and Paleontologists and Mineralogists, Special Publication 42, p. 109–124, https://doi.org/10.2110/pec.88.01.0109.
- Primm, J.W., Johnson, C.L., and Stearns, M., 2018, Basinaxial progradation of a sediment supply driven distributive fluvial system in the Late Cretaceous southern Utah foreland: Basin Research, v. 30, p. 249–278, https://doi .org/10.1111/bre.12252.
- Roberts, E.M., 2007, Facies architecture and depositional environments of the Upper Cretaceous Kaiparowits Formation, southern Utah: Sedimentary Geology, v. 197, p. 207–233, https://doi.org/10.1016/j.sedgeo.2006.10.001.
- Roberts, E.M., Deino, A.L., and Chan, M.A., 2005, ⁴⁰Ar/³⁹Ar age of the Kaiparowits Formation, southern Utah, and correlation of contemporaneous Campanian strata and vertebrate faunas along the margin of the Western Interior Basin: Cretaceous Research, v. 26, p. 307–318, https://doi.org/10.1016/j.cretres.2005.01.002.
- Roberts, L.N.R., and Kirschbaum, M.A., 1995, Paleogeography and the Late Cretaceous of the Western Interior of middle North America: Coal distribution and sediment accumulation: U.S. Geological Survey Professional Paper 1561, 115 p., https://doi.org/10.3133/pp1561.
- Robinson, R.A.J., and Slingerland, R.L., 1998, Grainsize trends, basin subsidence and sediment supply in the Campanian Castlegate Sandstone and equivalent conglomerates of central Utah: Basin Research, v. 10, p. 109–127, https://doi.org/10.1046/ j.1365-2117.1998.00062.x.
- Rountree, J.K., 2011, Evaluating the role of sediment supply in the development of foreland basin fill: An example from a low-accommodation clastic wedge in the Cordilleran Foreland Basin, Mesa Verde Group, Utah-Colorado [M.S. thesis]: Golden, Colorado, USA, Colorado School of Mines, 150 p.
- Rust, C.B., 2019, Transregional sequence-stratigraphic correlation of the Maastrichtian Fox Hills Sandstone (CO, WY, SD, ND, MT): Insight into forced regressive shoreline development in the North American Cordilleran Foreland Basin [M.S. thesis]: Anchorage, Alaska, USA, University of Alaska Anchorage, 131 p.
- Schwendeman, K.M., 2011, Sequence stratigraphy of the Upper Cretaceous, Castlegate condensed section through Iles Formation, Piceance Basin, northwestern Colorado [M.S. thesis]: Boulder, Colorado, USA, University of Colorado Boulder.
- Seymour, D.L., and Fielding, C.R., 2013, High resolution correlation of the Upper Cretaceous stratigraphy between the Book Cliffs and the western Henry Mountains syncline, Utah, U.S.A: Journal of Sedimentary Research, v. 83, p. 475–494, https://doi.org/10.2110/ jsr.2013.37.
- Shanley, K.W., and McCabe, P.J., 1994, Perspectives on the sequence stratigraphy of continental strata: AAPG Bulletin, v. 78, p. 544–568, https://doi.org/10.1306/ BDFF9258-1718-11D7-8645000102C1865D.
- Shanley, K.W., and McCabe, P.J., 1995, Sequence stratigraphy of Turonian-Santonian strata, Kaiparowits Plateau, southern Utah, USA: Implications for regional correlation and foreland basin evolution, in Van Wagoner, J.C., and Bertam, G.T., eds., Sequence Stratigraphy of Foreland Basin Deposits: AAPG Memoir, v. 64, p. 103–136.
- Shephard, G.E., Müller, R.D., Liu, L., and Gurnis, M., 2010, Miocene drainage reversal of the Amazon River driven by plate-mantle interaction: Nature Geoscience, v. 3, p. 870– 875, https://doi.org/10.1038/ngeo1017.
- Spasojević, S., Liu, L., and Gurnis, M., 2009, Adjoint models of mantle convection with seismic,

- plate motion, and stratigraphic constraints: North America since the Late Cretaceous: Geochemistry, Geophysics, Geosystems, v. 10, https://doi.org/10.1029/2008GC002345.
- Steckler, M.S., and Watts, A.B., 1978, Subsidence of the Atlantic-type continental margin off New York: Earth and Planetary Science Letters, v. 41, p. 1–13, https:// doi.org/10.1016/0012-821X(78)90036-5.
- Tanck, G.S., 1997, Distribution and origin of organic carbon in the Upper Cretaceous Niobrara Formation and Sharon Springs Member of the Pierre Shale, Western Interior, United States [Ph.D. thesis]: Tucson, Arizona, USA, The University of Arizona.
- Tindall, S.E., Storm, L.P., Jenesky, T.A., and Simpson, E.L., 2010, Growth faults in the Kaiparowits Basin, Utah, pinpoint initial Laramide deformation in the west-

- ern Colorado Plateau: Lithosphere, v. 2, p. 221–231, https://doi.org/10.1130/L79.1.
- Tufano, B.C., and Pietras, J.T., 2017, Coupled flexural-dynamic subsidence modeling approach for retro-foreland basins: Example from the Western Canada Sedimentary Basin: Geological Society of America Bulletin, v. 129, p. 1622– 1635, https://doi.org/10.1130/B31646.1.
- Varban, B.L., and Guy Plint, A., 2008, Sequence stacking patterns in the Western Canada foredeep: influence of tectonics, sediment loading and eustasy on deposition of the Upper Cretaceous Kaskapau and Cardium formations: Sedimentology, v. 55, p. 395–421, https://doi.org/10.1111/j.1365-3091.2007.00906.x.
- Wiechman, M.L., 2013, Basin-scale sequence stratigraphy and distribution of depositional and mechanical units in the middle and upper Williams Fork Formation, Picean-

- ce Basin, Colorado [M.S. thesis]: Golden, Colorado, USA, Colorado School of Mines, 189 p.
- Yonkee, W.A., and Weil, A.B., 2015, Tectonic evolution of the Sevier and Laramide belts within the North American Cordillera orogenic system: Earth-Science Reviews, v. 150, p. 531–593, https://doi.org/10.1016/ j.earscirev.2015.08.001.

SCIENCE EDITOR: ROB STRACHAN ASSOCIATE EDITOR: MICHAEL SMITH

Manuscript Received 16 July 2020 Revised Manuscript Received 27 January 2021 Manuscript Accepted 24 March 2021

Printed in the USA